POLITECNICO
DI TORINO

Master’s Degree in Mechanical Engineering

Department of Mechanical and Aerospace Engineering

Master’s Degree Thesis

Modeling of The Fatigue Behavior of Micro-Switch

Supervisors:
Prof. BRUSA EUGENIO
Prof. DELPRETE CRISTIANA

Candidate:
CUI GUIYANG

March 2021

Abstract

This thesis describes the suspended electrode's fatigue behavior in the RF-MEMS, mainly investigating the effect of temperature on this behavior; this is because the electric filed bends up and down the suspended electrode, while the Joule effect induces heating as a consequence. Firstly, the materials for the suspended electrode design are listed with their corresponding mechanical properties. Then, the damage mechanism of fatigue of the suspended electrode is discussed, mainly including the two relationships, the one between the temperature and the stress, and the other between the temperature and the fatigue strength. Due to the importance of thermal expansion in the fixed-fixed microstructure, the compressive stress caused by thermal conditions will be the critical point in our study, coupled with the residual stress, thereby predicting the fatigue life of the suspended electrode. Finally, simulation models will be used to determine the conclusion of this study.

Keywords: Mechanical design, fatigue life, buckling, thermal stresses, RF-MEMS

List of Figures

List of Tables

Contents

1. Introduction

At present, the RF-MEMS (Radio-frequency micro-electro-mechanical system) switch has become a research hotspot in science and technology. RF MEMS refers to radiofrequency microwave structures, devices, monolithic integrated subsystems, etc., that are realized by MEMS/NEMS technology micro-nano fine manufacturing. It has the advantages of miniaturization, low power consumption, low cost, integration, etc. Therefore, the RF-MEMS has been widely used in many fields. For example, it has gradually been widely used in military and civilian fields, including personal communications, such as mobile phones, PDA (Personal Digital Assistant), portable computer data exchange; Airborne and shipborne transceivers and satellite communication terminals, GPS receivers, etc.; information-based combat command, battlefield communications, miniaturized satellite communications systems, phased array radars, etc.

Italy FBK provides the technology used to implement the RF-MEMS devices and networks discussed in this chapter [1]. It is based on a surface micromachining process on a 4-inch silicon or quartz wafer. There are two buried layers available, namely a high-resistivity/low-resistivity channel layer suitable for DC replacement lines and electrodes, and an aluminum-based multi-metal layer suitable for RF signals. Two electroplated gold layers can realize actual MEMS devices and use sacrificial layers to define floating movable parts. The following two figures briefly describe the eight standard FBK RF-MEMS processes.

Specifically, Figure 1 sequentially describes the following operations:

1) The switch is manufactured using a 4-inch silicon substrate.
2) A silicon oxide layer is deposited on the wafer.
3) A high-resistivity or low-resistivity polysilicon is implanted onto the wafer to complete the first mask. The silicon oxide layer covers the entire wafer.

4) It is opened at the place that needs to be in electrical contact with the underlying polysilicon, thus completing the second mask.

5) The aluminum-based multi-metal layer is sputtered onto the wafer and then patterned to complete the third mask.

6) The silicon oxide layer covers the entire wafer, and holes are opened at the places that need to be in electrical contact with the underlying multi-metal layer to complete the fourth mask.

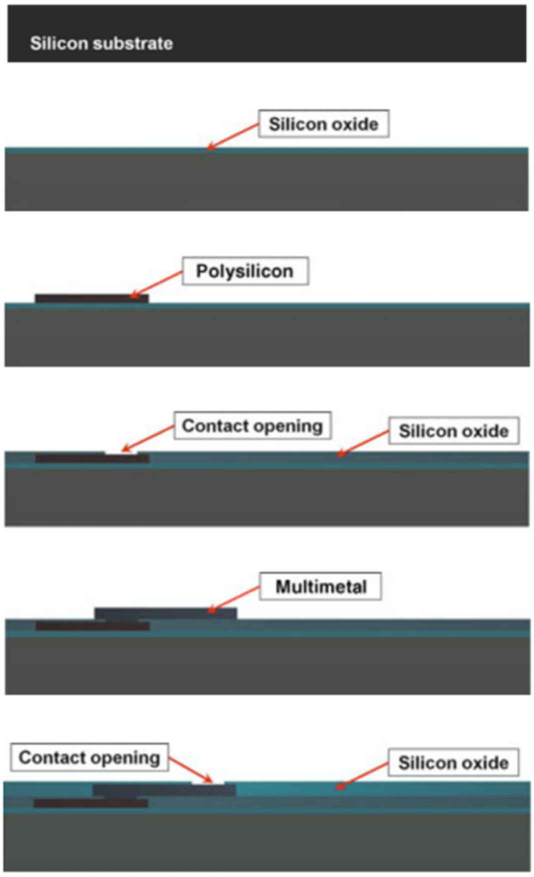

Fig. 1 The standard eight-mask RF-MEMS process A [1]

Figure 2 sequentially describes the following operations:

7) The thin gold layer is evaporated onto the contact opening above the multi-metal layer to complete the fifth mask.

8) Where the sacrificial layer is patterned, the microstructure is suspended to complete the sixth mask.

9) The first gold layer is electroplated to define lines, pads, anchors and suspended deformable structures, which completes the seventh mask.
10) The second gold layer is electroplated, and defines a part that means a harder microstructure, that is, the eighth mask is completed.
11) The sacrificial layer is removed, thereby releasing the suspended the RF-MEMS structure.

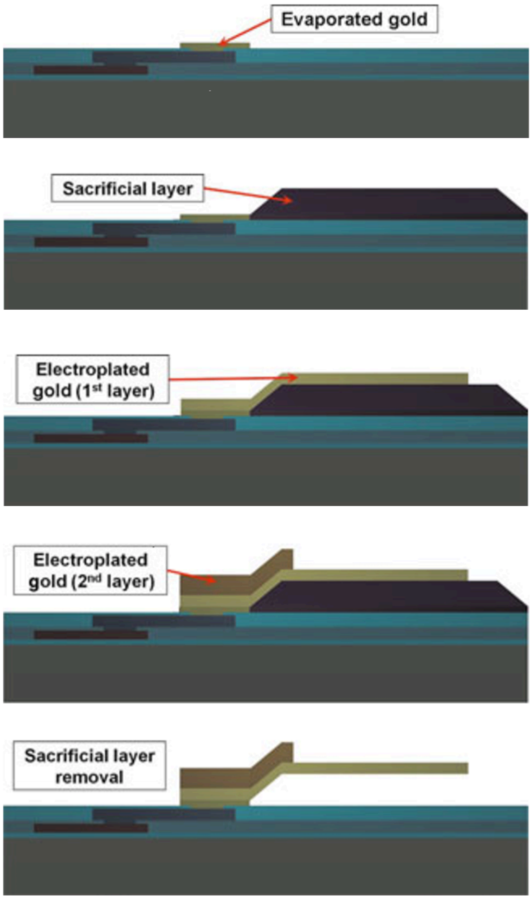

Fig. 2 The standard eight-mask RF-MEMS process B [1]

Generally, the RF-MEMS can be divided into two types, namely ohmic switch and capacitive switch, and the working principles of the two types will be briefly described later.

The following Figure 3 shows a typical structure of an ohmic switch, which consists of a suspended electrode that can close or open the electrical path between RF port 1 and RF port 2 according to its position, that is, the rest position or pull-in position.

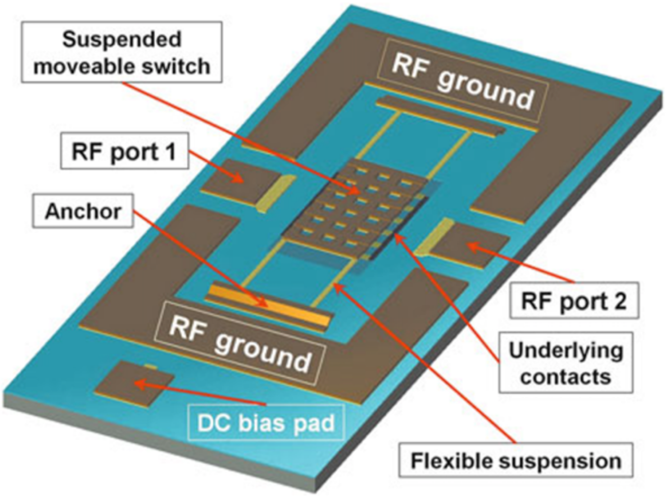

Fig. 3 Three-dimensional schematic of the RF-MEMS ohmic switch [1]

The following Figure 4 shows a typical structure of a capacitive switch. When the suspended electrode collapses on the substrate, it reaches a large capacitance, thereby realizing a low-impedance ground path for the RF signal. The movable electrode is a suspended gold membrane, and the four flexible suspensions are shaped like a meander in order to lower the elastic constant, thereby reducing the activation voltage of the device.

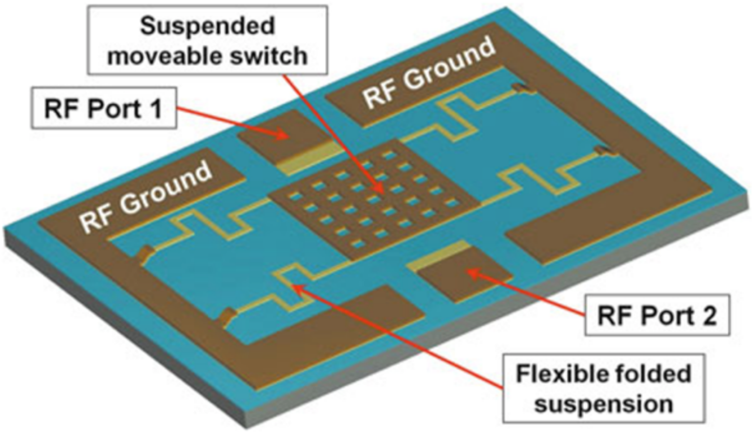

Fig. 4 Three-dimensional schematic of the RF-MEMS capacitive switch [1]

Compared with the ohmic switch, the capacitive switch is widely used. The working principle of the capacitive type will be described in detail. As shown in Figure 5, the typical implementation of a capacitor based on MEMS technology is based on two parallel electrodes, the one is fixed, and the other is movable. When there is no DC voltage between the movable electrode and the fixed electrode, the MEMS structure is in a static position. In this case, the distance between the two electrodes is the maximum, and the capacitance is the minimum. When a DC voltage is applied between the two electrodes, the top one starts to move towards the fixed plate due to electrostatic attraction, thus increasing the capacitance. When the applied DC voltage is larger than the pull-in voltage, the movable electrode contacts the lower electrode, in which the dielectric layer prevents an electrical short between two electrodes, its large capacitance to ground realizes a low-impedance path for the RF signal, which is shorted to ground, and consequently does not reach the output termination.

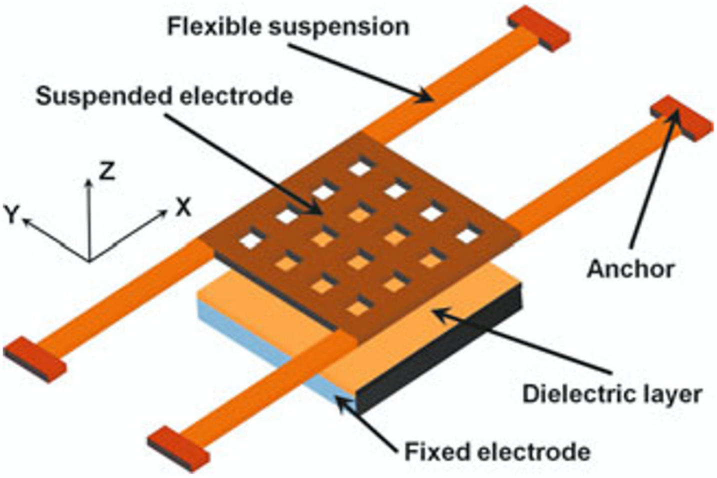

Fig. 5 RF-MEMS based on variable capacitor [1]

As the recent research shows, the RF-MEMS plays an important role in the field of 5G to express its potential, which is able to introduce a rather wide working frequency span from 10 MHz to 50 GHz. High working frequency means that the suspended electrode will undergo a high number of working cycles [2]. The suspended electrode tends to be failed because of overcoming the fatigue limit of the material. What’s more, common experience shows that there are temperature effects in RF-MEMS operation, so the microsystem's performance and life are significantly affected [3]. Most materials' mechanical characteristics are greatly influenced by the operating temperature, including ultimate strength, yield strength, fatigue limit, etc. The suspended electrode is the component that is influenced most by the operating condition, which means understanding the effect of the operation temperature on the suspended electrode's mechanical properties will help us predict the reliability of the microswitch device used in the radiofrequency application.

Nowadays, Au is the main material when designing a suspended electrode because of the excellent stability of material performance under high-temperature conditions. However, the price of material Au is around 51 €/g, almost 8500 times the price of material Cu, around $6.0*10^{-3}$ €/g. In order to reduce the cost of the RF-MEMS, this thesis aims to collect some possible material for the suspended electrode's design by comparing their mechanical properties with Au, especially focusing on the damage mechanism due to the condition of rising working temperature.

2. Materials of RF-switch

2.1 Materials

Selecting the proper material of the suspended electrode is the key performance deciding factor when designing the RF-MEMS. Ashby's material selection method is used to select the materials for different thin films in the switch design process [4]. High conductive metal should be given more consideration, and the material of the suspended electrode will affect the electrical and mechanical parameters of the RF-MEMS. There are some possible materials with high conductivity, including Au, Pt, Ti, Ni, Cr, Nb, and Al_2O_3.

A similar selection approach, which aims to optimize the choice of suspended electrode material and to minimize the intrinsic residual stress, provides similar possible materials, consisting of Al, Au, Ti, Cu, Pt, Ni, and Cr [5]. The material with a high thermal expansion coefficient and low Poisson's ratio provides better working performance by considering the operating voltage depending on Poisson's ratio and thermal expansion coefficient. Regarding the effective spring constant of the bridge, which strongly depends on the Young's modulus, a material with a lower Young's modulus will reduce the actuation voltage. After the computation and selection, SU-8, Al, and Au is a good choice, in which SU-8 is a brittle material, and some measures need to be adopted to improve this property and enhance the reliability [6].

To analyze the microbridge's displacement, the adopted approach is the change of the bridge material, including Poly-Si, Si, Cu, Al, and W [7]. Because of working conditions, the Si bridge requires the switches to be packaged. It will increase the whole process's cost, and metallic materials used in the RF-MEMS are a better selection. When designing the shape of the Micro-strip structure, rectangular cantilever and circular cantilever are compared by using different materials, consisting of Al, Au, Cr, Cu, Pd, Pt, Ti, and W [8]. It shows that the lightweight material like Al as structure provides good performance because of the decrease of the insertion and isolation losses. Compared with the circular shape, the rectangular shape gives a good deformation performance for less actuation voltage.

Compared with the beam's traditional structure, a novel step structure is introduced with many advantages, such as low pull-in voltage, low insertion loss, and high isolation [9]. This novel structure aims to reduce the gap between the beam and the signal line and provides a low spring constant, decreasing the pull-in voltage. To avoid the buckling effect, the critical stress of the membrane introduced by the electrostatic actuation is critical. This test has been done using different materials, including Au, Al, Pt, Ti, Cu, and Cr. Higher Young’s modulus means higher pull-in voltage required because of higher stiffness. By contrast, lower Young’s modulus means that the material tends to suffer a buckling effect. As a result, materials with moderate Young’s modulus are suitable for switches, such as Al and Au.

A novel multilayer film is introduced to improve the Au film's hardness, consisting of Au/Cu/Au. After the test in the atmosphere, the measurement indicates that the multilayer film's hardness is several times larger than the pure Au-film. Insertion loss and isolation perform better [10]. To reduce pull-in voltage and analyze the influence on the RF-MEMS performance introduced by structure parameters, a systematic comparison is carried out using several different material beams, including Al, Cu, Au, Mo, Ni, and Pt. Because pull-in voltage strongly depends on Young's modulus, more specifically, an increase in the Young’s modulus leads to an increase in pull-in voltage. The result shows that Al with the least Young’s modulus has the least pull-in voltage, which means this material will be the most suitable material for designing the beam [11]. To find the best choice for the bridge, a static analysis of the bridge has been carried out by varying the material including Ni, Cu, Al, and Au. this comparison indicates that the Al microbridge is the best choice with a low price a low needed voltage [12].

According to these papers, a list of possible materials used in suspended electrodes can be present in the following table. In this thesis, the pure metallic bridge will be mainly discussed.

Symbol	Chemical Name
Au	Gold
Pt	Platinum
Ti	Titanium
Ni	Nickel
Al	Aluminum
Cu	Copper
W	Tungsten
Pd	Palladium
Mo	Molybdenum
Rh	Rhodium

Table 1 List of material

2.2 Materials properties

The fatigue phenomenon is introduced by cyclic loading conditions, in which the strength of the material is reduced. Damage evolution of fatigue failure mainly includes three stages, a crack's nucleation, a crack's growth, and the final fatigue crack, respectively. At the first stage, fatigue cracks are “small,” the material is in stable condition. However, at the second stage, fatigue cracks are “large” that material is unstable when the length of cracks becomes critical, which means stress that is lower than yield and ultimate tensile stress can induce the fatigue rupture.

To analyze fatigue damage, yield strength, ultimate tensile strength, and fatigue limit are essential and fundamental properties. It is much better if the S−N curve is provided since it clearly presents the number of cycles to failure for each specimen concerning the stress amplitude. It is the most commonly used method to obtain standard ultimate tensile strength ($R_{m,N}$) and standard yield strength ($R_{e,N}$) from the material dictionary. We can then use the corresponding coefficient to modify the result, which stands for the effects affecting the material behavior in terms of strength. The coefficient terms are related to the size of the mechanical component ($K_{d,m}$, $K_{d,e}$) and material processing (K_A). The corresponding formula is shown in the following.

$$R_m = K_{d,m} * K_A * R_{m,N} \tag{1.}$$

$$R_e = K_{d,e} * K_A * R_{m,N} \tag{2.}$$

The corresponding fatigue limit is also obtained by the following formula by considering the fatigue coefficient $f_{w,\sigma}$.

$$\sigma_{D-1}^{tc} = f_{w,\sigma} * R_m \tag{3.}$$

Since there is a temperature effect on RF-MEMS in the real working condition, the related temperature coefficient is introduced by the following formula.

$$\sigma_{D-1,T} = K_{T,D} * \sigma_{D-1} \tag{4.}$$

According to "Material Handbook," the corresponding properties of each material are collected in the following table, in which these properties are obtained by testing at 293.15 K [13].

Symbol	Tensile ultimate strength [MPa]	Yield strength [MPa]
Au	127	n.a.
Pt	137.9	70
Ti	220	140
Ni	462	148
Al	110	55
Cu	221	69
W	980	750
Pd	227.5	65
Mo	435	345
Rh	758.6	68

Table 2 Properties of material

The suspended electrode's geometrical parameters are 500μm*35μm*2μm. Because these values are similar to the values used in the paper [14], and it is easy to compare when we have any result. Firstly, technological size factor $K_{d,m}$ will be computed through the FKM method with these geometrical parameters, in which d_{eff} is 2μm, and $d_{eff,N,m}$ is 40mm. The corresponding $K_{d,m}$ is 1. Secondly, anisotropy factor K_A depends on the direction of milling and/or forging. The corresponding K_A for each material is shown in the following table.

Symbol	Tensile ultimate strength [MPa]	K_A
Au	127	1
Pt	137.9	1
Ti	220	0.95
Ni	462	0.9
Al	110	1
Cu	221	0.95
W	980	0.8
Pd	227.5	0.95
Mo	435	0.9
Rh	758.6	0.85

Table 3 List of anisotropy factor

With technological size factor $K_{d,m}$ and anisotropy factor K_A, the modified tensile ultimate strength R_m is allowed to compute, which is shown in the following table. Besides, in order to determine the bending fatigue limit, we can use the approximate coefficient which describes the relationship between the modified tensile ultimate strength and the bending fatigue limit, which is equal to 0.5.

Symbol	Modified tensile ultimate strength [MPa]	Bending fatigue limit at 293.15 K
Au	127	63.5
Pt	137.9	68.95
Ti	209	104.5
Ni	415.8	207.9
Al	110	55
Cu	209.95	104.975
W	784	392
Pd	216.125	108.0625
Mo	391.5	195.75
Rh	644.81	322.405

Table 4 List of modified tensile ultimate strength and bending fatigue limit at 293.15K

With the Shigley theory, at least the fatigue life under axial loading is around 85% of that in bending loading which means the bending fatigue limit is higher than the tensile fatigue limit, in which the corresponding formula is shown as the following:

$$\sigma_{D-1}^{tc} = 0.85 * \sigma_{D-1}^{b} \tag{5.}$$

With this formula, the corresponding tensile fatigue limit can be obtained as the following table:

Symbol	Tensile fatigue limit at 293.15 K
Au	53.975
Pt	58.6075
Ti	88.825
Ni	176.715
Al	46.75
Cu	89.22875
W	333.2
Pd	91.853125
Mo	166.3875
Rh	274.04425

Table 5 List of tensile fatigue limit at 293.15K

Due to the limitations of size and microstructure, the mechanical properties cannot be simply derived from the mechanical properties of their bulk counterparts. Therefore, it is necessary to study the influence of scale effect and microstructure on the mechanical behavior of films through experiments. When the components are as small as micro-nano size, the mechanical and physical properties of these materials themselves will change significantly, and strong size effects and surface effects will appear. The RF-MEMS components are usually represented by thin films with structural functions, which makes mechanical characterization more complicated; currently there is no standard procedure to determine the properties and fatigue performance of a given component. In order to understand these behaviors systematically, we collect some typical examples in the following.

2.2.1 Au microbeams test

In order to analyze the mechanical fatigue behavior of gold microbeams, a dedicated device has been created which is able to produce alternate loading to simulate the real working condition [15]. Fatigue tests have been done by using bending loadings and alternate loadings respectively. In the tensile fatigue test, three different levels of tensile mean stress were produced at 50, 60, and 65MPa, respectively, and the dimensions of the components used in this test include 27,7um in length, 11,2um in width and 1,9um in thickness.

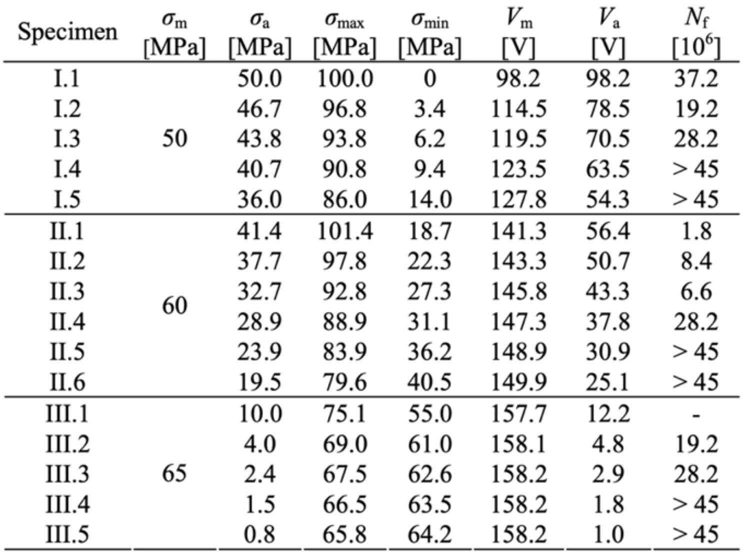

Specimen	σ_m [MPa]	σ_a [MPa]	σ_{max} [MPa]	σ_{min} [MPa]	V_m [V]	V_a [V]	N_f [10^6]
I.1	50	50.0	100.0	0	98.2	98.2	37.2
I.2		46.7	96.8	3.4	114.5	78.5	19.2
I.3		43.8	93.8	6.2	119.5	70.5	28.2
I.4		40.7	90.8	9.4	123.5	63.5	> 45
I.5		36.0	86.0	14.0	127.8	54.3	> 45
II.1	60	41.4	101.4	18.7	141.3	56.4	1.8
II.2		37.7	97.8	22.3	143.3	50.7	8.4
II.3		32.7	92.8	27.3	145.8	43.3	6.6
II.4		28.9	88.9	31.1	147.3	37.8	28.2
II.5		23.9	83.9	36.2	148.9	30.9	> 45
II.6		19.5	79.6	40.5	149.9	25.1	> 45
III.1	65	10.0	75.1	55.0	157.7	12.2	-
III.2		4.0	69.0	61.0	158.1	4.8	19.2
III.3		2.4	67.5	62.6	158.2	2.9	28.2
III.4		1.5	66.5	63.5	158.2	1.8	> 45
III.5		0.8	65.8	64.2	158.2	1.0	> 45

Table 6 Stress level and actuation voltages used for Au microbeams test [15]

According to Goodman-Smith theory, the figure shows the trend line derived from the experimental results, which help us to determine the values roughly, including the ultimate stress (about 110MPa), yield stress (about 75MPa) and tensile fatigue limit (about 60MPa). According to Shigley theory, the estimated bending fatigue limit in this test is around 70 MPa, which is higher than the bending fatigue limit obtained in the previous chapter (around 63.5MPa), and mainly because the fatigue limit of the metal micro-film has changed significantly compared with the macro-film.

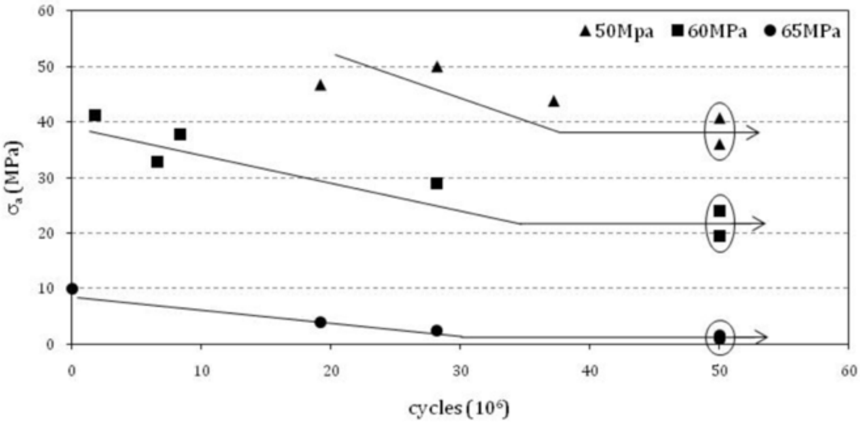

Fig. 6 S-N curve of Au microbeams test [15]

2.2.2 Cu microbeams test

Since copper is a nonferrous metal material, it presents a continuously decreasing S-N responses and the fatigue limit cannot be obtained. In order to determine an effective fatigue limit, a number of cycles must be specified such as 1*10^8 or 5*10^8 loading cycles.

The most important steps in the manufacturing of integrated circuits are ion implantation, diffusion, epitaxial growth, chemical vapor de position/physical vapor deposition and their variations, wet and dry etching, sputtering, evaporation, and electrodeposition of metals, and specifically the suspended electrode can be obtained by the using of electrodeposition of the metal layer [1]. To study the effect of manufacturing methods on the properties of thin film materials, the samples used in this test are manufactured by rolling and electroplating [16]. Although specimen by the rolling process is better than by electrodeposition process, we concentrate on the behavior of the second specimen because it has a manufacturing process similar to that of the RF-MEMS. The relationship between the stress amplitude and the number of cycles to failure is obtained to plot the life-stress curve, in which this relationship is expressed by Basquin's equation.

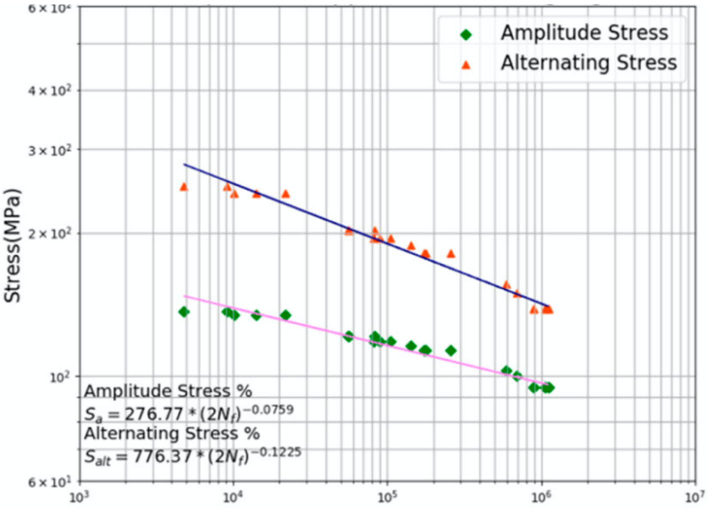

Fig. 7 S-N curve of Cu microbeams test [16]

Since the mean stress during this test is not zero, and Goodman line can help us fine an effective stress amplitude with non-mean stress that produces the same damage by projecting along this line in the mean stress & stress amplitude diagram. The corresponding tensile fatigue limit is 276.77 MPa obtained from the stress amplitude and 776.37 MPa obtained from the effective stress, respectively. Compared with the bulk copper characteristics, the tensile fatigue limit of copper thin films is almost ten times higher than of bulk copper. This is mainly because the mechanical properties of thin films cannot be simply derived from those of their bulk materials, we need to pay more attention on the effect of component size, fabricating method, and testing method and so on. It is necessary to set up a standard test procedure which helps us to obtain the more accurate mechanical properties of the microstructure. In our thesis, we will not talk about this issue and we will focus on the damage mechanism and temperature effect on their behavior.

2.2.3 Ni microbeams test

Because of the advantages of low-residual stress and high mechanical strength, Ni microbeam manufactured by electroplating is a possible choice when designing the RF-MEMS. The aim of this paper is to study the effect of stress gradient on fatigue behavior in notched components and unnotched components under bending loads [17]. In presence of a gradient of stress, which means the stress on the surface is the maximum stress but not control the fatigue behavior. The effective stress with the lower value than maximum stress is the key element which govern fatigue behavior. During this test, we will focus on the S-N curve of unnotched components by applying bending load. The cross section of microbeams used in this test include 26μm in thickness and 250μm in width.

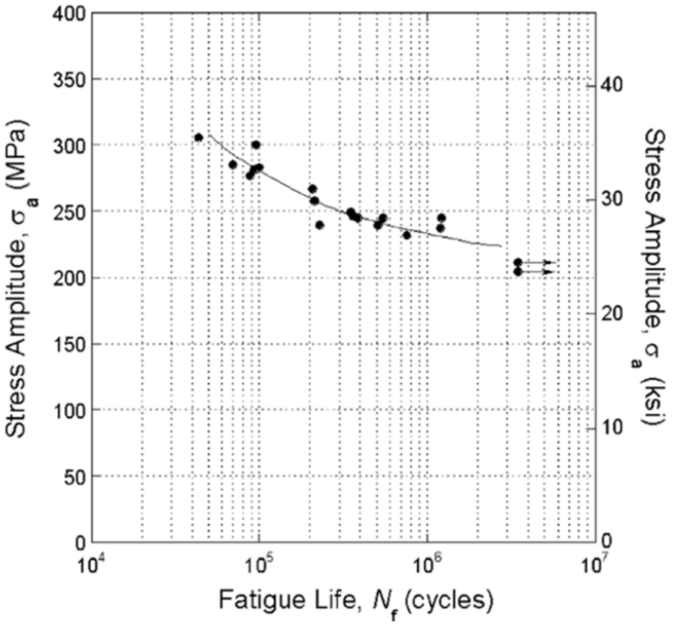

Fig. 8 S-N curve of Ni microbeams test [17]

This Ni microbeam under fully reversed bending load which R is equal to -1. From this diagram, we can obtain the bending fatigue limit around 208 MPa, which is similar to the value calculated in the previous chapter.

2.2.4 Al microbeams test

An important step in the manufacture of the RF-MEMS is to form a suspended microbeam [11]. Generally, the beam is made of gold due to its high electrical conductivity and chemical inertness. However, due to the poor adaptability of gold to chemical etching and the deformation of the beam under residual mechanical stress, the manufacturing process becomes complicated. Aluminum and its alloys are considered promising alternatives [18].

The purpose of this research is to statistically evaluate the fatigue life data obtained from the cantilever plane bending fatigue test, which is suitable for 99% commercial pure general-purpose aluminum plates produced by cold rolling; and establish S-N curve, to estimate the fatigue life of these materials at 12 different reliability levels from R = 0.01 to 0.99 [19]. In this study, commercial purity cold rolled aluminum plates were used. The following tables provide the related chemical composition and standard symbols. Test samples were prepared by cutting AA1100 (99.4% pure) and AA1050 (99.6% pure) cold-rolled aluminum sheets into dimensions of 25mm×200mm×3mm in the rolling direction (RD) and long transverse direction (LT).

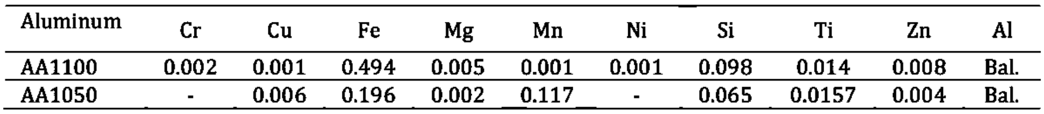

Aluminum	Cr	Cu	Fe	Mg	Mn	Ni	Si	Ti	Zn	Al
AA1100	0.002	0.001	0.494	0.005	0.001	0.001	0.098	0.014	0.008	Bal.
AA1050	-	0.006	0.196	0.002	0.117	-	0.065	0.0157	0.004	Bal.

Table 7 Chemical composition of aluminum sheets [19]

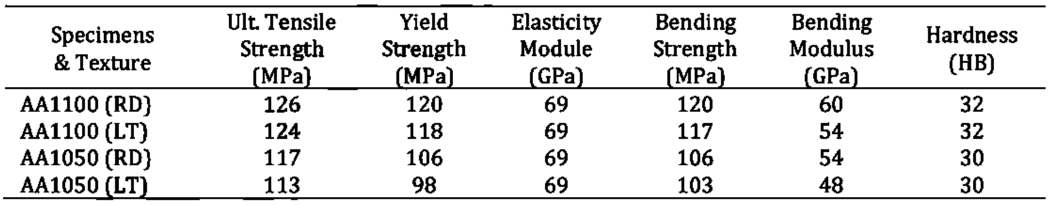

Specimens & Texture	Ult. Tensile Strength (MPa)	Yield Strength (MPa)	Elasticity Module (GPa)	Bending Strength (MPa)	Bending Modulus (GPa)	Hardness (HB)
AA1100 (RD)	126	120	69	120	60	32
AA1100 (LT)	124	118	69	117	54	32
AA1050 (RD)	117	106	69	106	54	30
AA1050 (LT)	113	98	69	103	48	30

Table 8 Mechanical properties of aluminum sheets [19]

Since aluminum material does not exhibit well-defined fatigue limit, in order to evaluate the fatigue test results, the fatigue strength corresponding to 10^7 cycles is used as the effective fatigue limit. The following equation is used to evaluate the fatigue test data, which is a simplified Basquin function, where σ_a is the stress amplitude (fatigue strength), N_f is the failure cycle causing failure, and A and b are constants.

$$\sigma_a = A * {N_f}^b \tag{6.}$$

The following figure 9 presents the fatigue test result with a reliability level R = 0.99, and four corresponding Basquin formulas are provided as shown in the following.

For AA1100(RD):

$$\sigma_a = 307.52 * {N_f}^{-0.211} \tag{7.}$$

For AA1100(LT):

$$\sigma_a = 199.50 * {N_f}^{-0.188} \tag{8.}$$

For AA1050(RD):

$$\sigma_a = 453.33 * {N_f}^{-0.245} \tag{9.}$$

For AA1050(LT):

$$\sigma_a = 426.73 * {N_f}^{-0.263} \quad (10.)$$

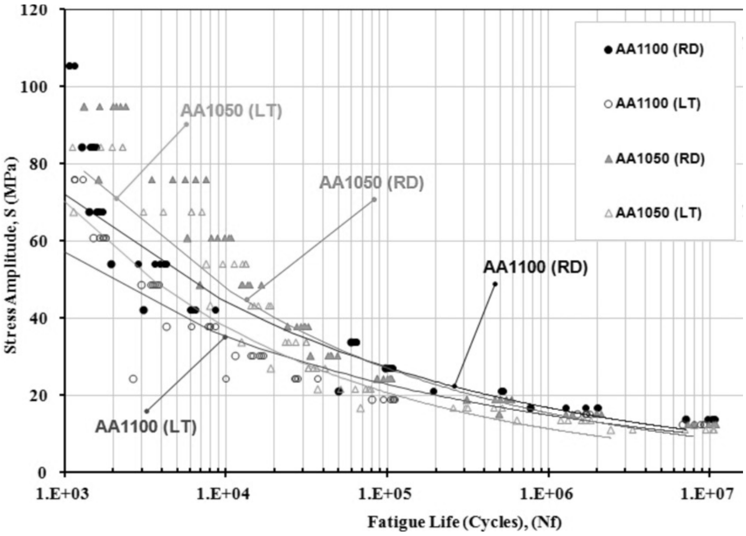

Fig. 9 S-N curve of Al specimens tests at R=0.99 reliability [19]

The following figure 10 presents the fatigue test result with a reliability level R = 0.50, and four corresponding Basquin formulas are provided as shown in the following.

For AA1100(RD):

$$\sigma_a = 330.38 * {N_f}^{-0.206} \quad (11.)$$

For AA1100(LT):

$$\sigma_a = 274.63 * {N_f}^{-0.209} \quad (12.)$$

For AA1050(RD):

$$\sigma_a = 543.59 * {N_f}^{-0.249} \quad (13.)$$

For AA1050(LT):

$$\sigma_a = 499.89 * {N_f}^{-0.255} \quad (14.)$$

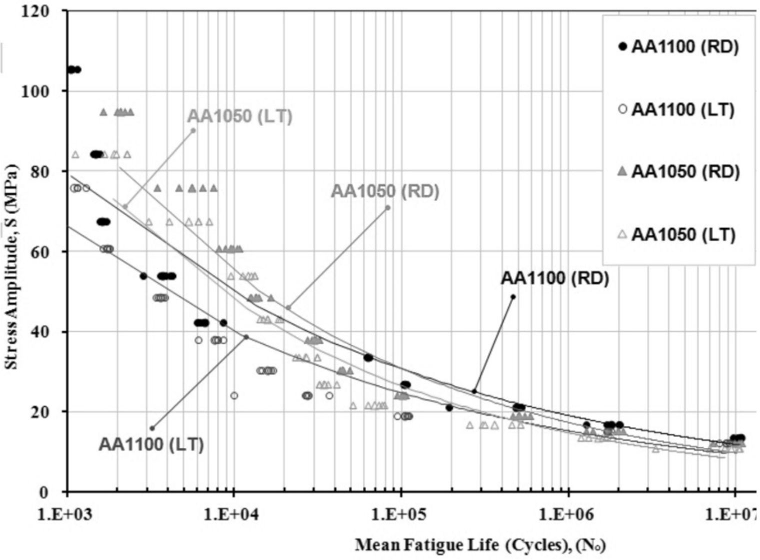

Fig. 10 S-N curve of Al specimens tests at R=0.50 reliability [19]

Normally, the standard fatigue limit σ_D is determined by the S-N curve with 50% survival probability. We will end the discussion about the fatigue limit from the published research and move to the study of the damage mechanism of fatigue behavior.

3. Damage mechanism of fatigue

The fatigue strength of the sample is a complex phenomenon, which will be affected and changed by many factors. The factors that affect the fatigue life of specimens can be roughly divided into three categories, including physical effects, metallurgical effects and load effects. During this part, we will provide the general method for predicting fatigue life by considering the temperature effect.

Three different technologies are typically used in fatigue life prediction of RF-MEMS devices, including stress-life methods, strain-life methods, and fracture crack growth methods. The most commonly used method is based on the stress-life method, which relies on evaluating the average stress and alternating stress in the studied microstructure. The first and most detailed study on fatigue is attributed to Wohler. Based on the stress-life method, fatigue is identified and quantified based on the relationship between alternating stress and the number of failure cycles, usually called the Wohler curve or S-N curve. This method does not distinguish between initiation and propagation but addresses the total lifetime of the components.

During the stress-life method, the first thing for us is to analyze the characteristic of stresses induced by operation. For example, if there is a constant stress excitation applied on the microstructure, we can determine the fatigue life by using S-N curve directly, and this damage is induced by single stress amplitude. By contrast, if the excitation applied on the microstructure is variable, the following three steps can help us to determine the fatigue life which is commonly known as Miner's Rule based on the concept of cumulative damage, including the counting of cycles of each stress amplitude, the computation of damage induced by each stress amplitude, and the sum of damage cumulation.

When the stress ration R is not -1 which means we need to take account into the presence of the mean stress by using Goodman line to obtain an effective stress amplitude with non-mean stress producing the same, in which the tensile mean stress affect fatigue life and the shear mean stress does not affect fatigue life. If the stress is tensile stress or bending stress without any coupling, we can determine their fatigue life by comparing their corresponding fatigue limit respectively. However, if several stress components are superposed, in presence of coupling of tensile stress and/or bending stress and/or shear stress, we need to find the relationship between these coupling stress to obtain an equivalent stress which produce the same damage. According to Shigley's suggestion, the relation between these stresses is described as the following formula:

$$\sqrt{(\sigma_a^f + \frac{\sigma_a^t}{0.85})^2 + 3\tau_a^2} = \sigma_{a,eq} \tag{15.}$$

in which σ_a^f is bending stress due to flexural behavior, σ_a^t is axial stress due to tensile and compressive load, τ_a is shear stress due to torsion behavior, and $\sigma_{a,eq}$ is equivalent stress used to compared with bending fatigue limit.

3.1 Stress analysis

Back to the RF-MEMS, we will analyze the deformation of suspended electrode by the applied voltage between the two electrodes. In order to concentrate on the analysis of temperature effect on fatigue behavior, the notch effect will be ignored, simple geometry of the suspended electrode is considered, and the most critical area is usually the center of the beam subjected to the largest deformation [20]. Besides, when the deformation of the suspended electrode is greater than the thickness, the non-linear effect of the suspended electrode will be significant due to the coupling of the bending effect and stretching effect.

Due to the clamped-clamped structure, the suspended electrode becomes statically indeterminate structure that the number of degrees of freedom is more than six, which means the suspended electrode tends to present the residual stress within the RF-MEMS after microfabrication process. The main reason is the different thermal expansion coefficient of gold and chrome used in the RF-MEMS, causing a residual strain distribution after a removal process of the sacrificial layers. To determine the residual stress, usually the experimental detection of the first resonance frequency plays an important role in this dynamic experiment. A low residual stress in RF-MEMS is generally desirable because switches with zero residual stress are more subject to problems, such as buckling.

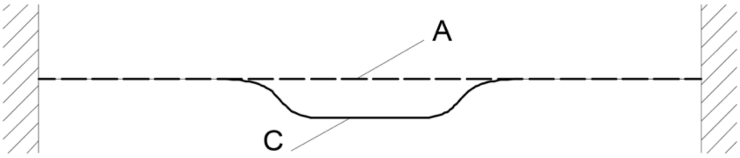

Fig. 11 Initial position and pull-in position of the suspended electrode

To simplify a single switch on/off operation process, we will focus on the initial position where the suspended electrode subjects to the minimum stress, and pull-in position where it subjects to the maximum stress. The suspended electrode starts to move from the initial position which is switch off position as line A shown in Figure 11, and then reach the pull-in position which is switch on position as line B shown in Figure 11, and finally return to the starting point. During this operation cycle, the corresponding minimum stress and maximum stress can be expressed as σ_{min} and σ_{max}, respectively, in which σ_{min} is the stress at the initial position as line A, and σ_{max} is the stress at the pull-in position as line B.

In order to calculate the fatigue life of the suspended electrode, the stress amplitude σ_a and mean stress σ_m are key parameters. For example, if the residual stress is not considered, at the initial position, the displacement is zero and the stretching effect and bending effect does not occur which means minimum stress is zero. With the minimum stress and maximum stress, the corresponding stress amplitude and mean stress are expressed in the following formulas:

$$\sigma_a = \frac{\sigma_{max} - \sigma_{min}}{2} \tag{16.}$$

$$\sigma_m = \frac{\sigma_{max} + \sigma_{min}}{2} \tag{17.}$$

For the suspended electrode in our thesis, it does not under fully reversed load, and the mean stress is not zero, and the stress ration R is not -1, which means that the effect of mean stress on the fatigue performance need to be considered. As a consequence, the equivalent stress amplitude for null mean stress needs to be introduced with producing the same damage.

The modified Goodman line is the most commonly used mean stress correction in industry and probably the most "popular" model with engineering field, and the equivalent stress amplitude can be expressed as a function of the mean stress and alternate stress, being the ultimate tensile strength a material constant; this means that for a given couple (S_m, S_a) there exists an equivalent condition (0, S_{ae}) (fully reversed loading) which provides the same number of cycles to failure as (S_m, S_a) [21].

$$\frac{S_m}{S_u} + \frac{S_a}{S_{ae}} = 1 \tag{18.}$$

In which, S_a (σ_a) is the stress amplitude, S_m (σ_m) is the mean stress, S_u (R_m) is the ultimate tensile strength, and S_{ae} (σ_{ae}) is the effective stress amplitude which is in the fully reversed loading conditions. In order to unify the symbols, the formula can be transformed into the following form:

$$\frac{\sigma_m}{R_m} + \frac{\sigma_a}{\sigma_{ae}} = 1, \qquad \sigma_m \geq 0 \tag{19.}$$

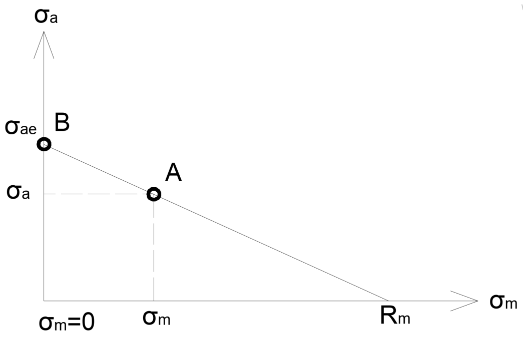

Fig. 12 Equivalent stress amplitude for null mean stress

In other words, the couple (σ_m, σ_a) and the couple (0, σ_{ae}) provide the same damage, and the fatigue life of the components under these two couples will be the same. Therefore, the stress of point B produces the same damage effect as the stress of point A does, and the corresponding formula used to determine the equivalent stress amplitude is expressed as the following:

$$\sigma_{ae} = \sigma_a * \left(\frac{R_m}{R_m - \sigma_m}\right), \quad \sigma_m \geq 0 \tag{20.}$$

3.2 Temperature effect

Joule heating describes the process where the energy of an electric current is converted into heat as it flows through a resistance. This also happens in the operation of the RF-MEMS device, since the voltage applied is needed to actuate the suspended electrode to bend in order to change the capacity.

In practice, the actuation frequency is quite high, and just like the micro switch is almost continuously heated, because the conduction process during the switch-off operation is not fast enough to transfer the heat stored in the microstructure [14]. According to Joule's first law, the heat per unit time developed in the wire is proportional to the resistance of the wire and to the square of the current. When a resistor of resistance R has a current I at voltage V, the power absorbed in the resistor is P expressed as the following.

$$Q = I^2 * R = \frac{V^2}{R} = V * I \tag{21.}$$

The Joule heat Q is dissipated by three modes of heat transfer, including convection mode Q_c, conduction mode Q_k, and radiation mode Q_r.

$$Q = Q_c + Q_k + Q_r \tag{22.}$$

The heat due to convection will be transferred out through natural convection, because there is no air flow in the immediate area of the RF-MEMS. The heat due to conduction can be determined by the Fourier's law because of characteristic of one-dimensional flow, where the temperature difference between two anchor end points will be the most important parameter. The heat due to radiation is closely related to the emissivity of the RF-MEMS surface and the temperature difference between the surface of the RF-MEMS and the surface of enclosure.

In our thesis, we will not discuss the relationship between the change of working temperature due to the joule effect and will focus on the effect of the change of temperature on the behavior of the suspended electrode.

In order to carry out this topic, there are some fundamental assumptions needed to be set up. For example, there are three phases for the describing the change of the working temperature, including phase 1 which is the initial working temperature, phase 2 which is the increase phase with time, and phase 3 which is the final working temperature in the balanced state.

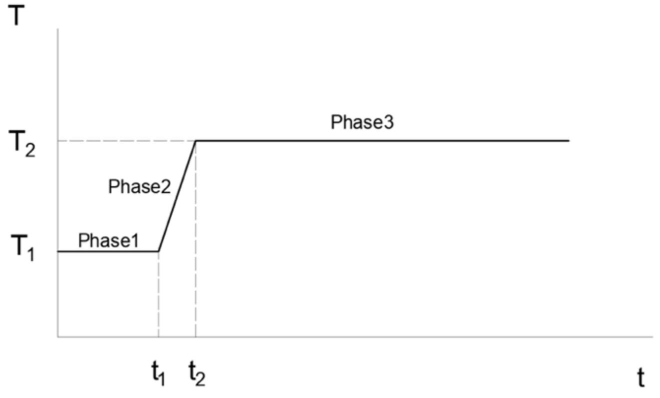

Fig. 13 Three phases for temperature change

$$\begin{cases} \text{Phase 1}: T = T_1, & 0 < t < t_1 \\ \text{Phase 2}: T = T_1 + \Delta T(t), & t_1 < t < t_2 \\ \text{Phase 3}: T = T_2, & t \geq t_2 \end{cases} \tag{23.}$$

In which, T_1 is room temperature 293.15K, T in phase 2 increases linearly or nonlinearly with time, and phase 3 is the state of dynamic equilibrium phase that the heat generated by the joule effect is equal to the heat transferred by the conduction process. Considering the total fatigue life of the suspended electrode and the properties of microstructure, we assume that the number of cycles to the dynamic equilibrium state can be ignored which means the final working temperature T_2 of the dynamic equilibrium is the key parameter in the following study.

3.2.1 Effects on Young's modulus

Young's modulus E is the initial part of the stress/strain curve, which describes the ability of a material to resist elastic deformation under load. It describes a material that retains its shape when it is stretched, pulled, twisted or compressed. When the material has a high modulus, the material can resist the initial force and recover well even under extreme strain. The ratio of stress to strain is Young's modulus, and Young's modulus can be considered as a measure of material stiffness. Stiffness determines the strength of the material, and measures the resistance to elastic deformation, while strength measures the stress that a material can withstand before permanent deformation or fracture occurs. When the temperature rises, the thermal vibration of the atom increases, which will cause the lattice potential energy and the curvature of the potential energy curve to change, so Young's modulus will also change. And as the temperature increases, the material will expand in volume.

Therefore, we know that the change of Young's modulus with temperature involves two aspects, one is the binding force of atoms, and the other is the volume of the material, which means that the relationship between Young's modulus and the temperature is relatively complicated. However, according to many experiments, it is observed that Young's modulus of several materials has a linear relationship. Normally, Young's modulus decreases when the temperature increase. Some examples are presented in the following to illustrate the change of Young's modulus with the change of temperature.

Gold film exhibites linear variation of the Young's modulus with the increasing temperature from 296K to 393K, in which Young's modulus decreases at 393K of 2% of the magnitude measured at room temperature [14]. To study the effect of temperature increasing on the

Young’s modulus, tests have been done under the temperature range from 293K to 373K by using several specimens with different thickness [22]. These specimens present the similar linear relationship between the Young’s modulus and the temperature, and the difference is that the specimen with higher thickness has the higher Young’s modulus at the same temperature and undergoes a greater drop in Young’s modulus with the same temperature range.

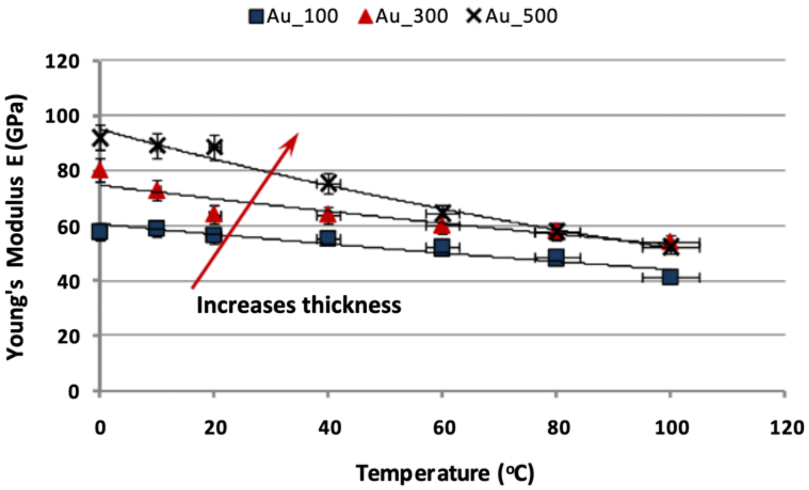

Fig. 14 Temperature effect on Young's modulus of Au [22]

To analyze the influence of the thermally grown oxidized Ni on the evolution of the Young’s modulus of Ni thin films with temperature, several specimens have been tested under the temperature range from 0 to 600°C to record the evolution of the Young’s modulus with temperature [23]. In higher temperature range from 360 to 600°C, these specimens present the similar evolution that can be expressed as a linear decrease of the Young’s modulus with the temperature. On the contrast, considering lower temperature range from 0 to 360°C, the presence of the NiO oxide layer on the Ni substrate plays an important role on the evolution of the Young’s modulus, and the evolution becomes nonlinear. It should be noted that between 0 to 100°C, the Young's modulus also shows an approximately linear trend.

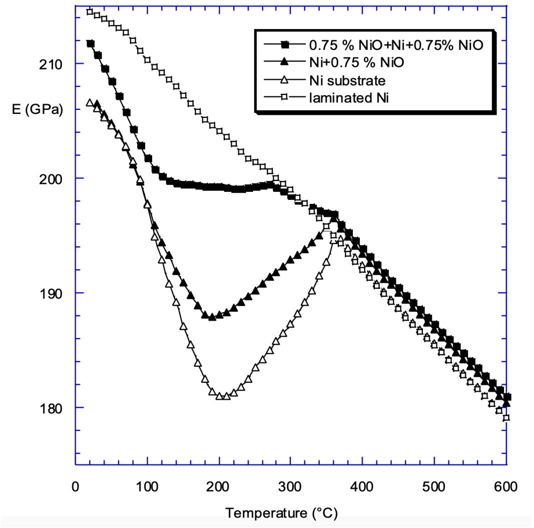

Fig. 15 Temperature effect on Young's modulus of Ni [23]

To predict the change of Young’s modulus of Aluminium with temperature, the corresponding tests have been carried out to demonstrate the approximatively linear relationship during the temperature range from -200 to 200°C [24]. The corresponding formula is given:

$$E(T) = 70 - 0.05 * T \tag{24.}$$

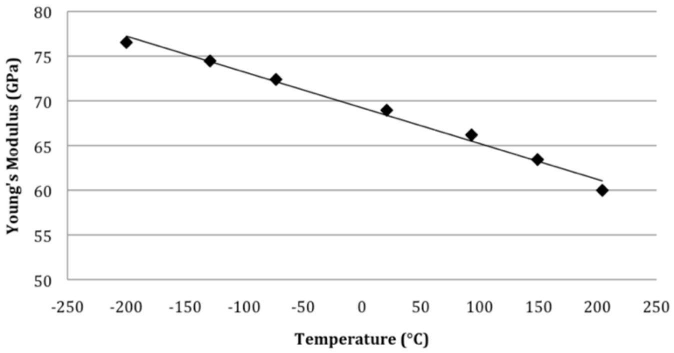

Fig. 16 Temperature effect on Young's modulus of Al [24]

To determine the correct relationship between Young’s modulus and temperature, many tests need to be carried out to find the approximative formula used to express this relationship. The effect of thickness, environment, the surface state of specimens should be considered during the test because these factors tend to play different roles in the evolution process.

Considering the linear relationship between Young's modulus and temperature, the general formula used to determine the modified Young's modulus is expressed normally as the following:

$$E(T) = E_0 + \Delta E * \Delta T \tag{25.}$$

In which, E_0 is the Young's modulus tested under the standard temperature, ΔE is the slope of the line, and ΔT is the temperature difference between the working temperature and the standard testing temperature. In our thesis, we assume the working temperature is the temperature in the state of dynamic equilibrium. Therefore, we can reasonably predict that an increase in temperature will directly lead to a decrease in Young's modulus, which in turn leads to a decrease in stress, because the stress is a function of Young's modulus. The reduction in stress has a possibility to lead to an increase in fatigue life.

3.2.2 Effects on the elongation of the suspended electrode.

Because of the fixed-fixed structure, the length of the suspended electrode is constant when the axis of this beam remains straight. When temperature increases, the thermal load is introduced. The axial thermal load can be obtained by the common model, and the corresponding formula is the following:

$$P_{thermal} = \alpha * \Delta T * E * A' \tag{26.}$$

In which, the area A' where the thermal load is applied is the cross-sectional area of the suspended electrode, is expressed as the following equation:

$$A' = W * t \tag{27.}$$

The corresponding compressive stress σ_c along axial direction can be expressed as the following:

$$\sigma_{compressive} = \frac{P_{thermal}}{A'} = \alpha * \Delta T * E \tag{28.}$$

During the real working condition, if the residual stress is considered, there will be three different cases concerning the compassion of the thermal stress and residual stress, which will influence the initial position of the suspended electrode in the following switch on/off cycles, including "$\sigma_r = \sigma_c$" case, "$\sigma_r > \sigma_c$" case and "$\sigma_r < \sigma_c$" case. It should be noted that the subscript c here means compressive stress, and subscript r here means residual stress.

Firstly, in the case of "$\sigma_r = \sigma_c$", there is no axial stress inside the suspended electrode when this electrode is at the initial position because the tensile residual stress is balanced by the thermal compressive stress. Besides, the vertical stress is zero because of the zero vertical displacements, which means the equivalent stress at this position is zero, and the axis of the suspended electrode keeps straight.

Secondly, in the case of "$\sigma_r > \sigma_c$", there is an equivalent tensile stress inside the suspended electrode because the tensile residual stress is greater than the thermal compressive stress. Due to this tensile effect inside the structure, the axis of the suspended electrode will keep straight at the initial position in the following switch on/off working cycles.

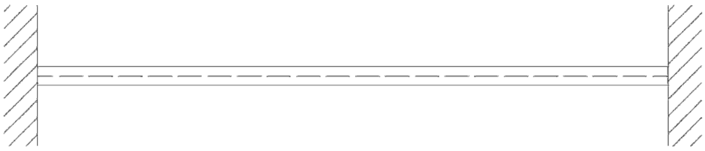

Fig. 17 Switch off position in case of $\sigma_r > \sigma_c$ and $\sigma_r = \sigma_c$

Finally, in the case of "$\sigma_r < \sigma_c$", which is a relatively complicated situation, there is equivalent compressive stress inside the suspended electrode because the thermal compressive stress is greater than the tensile residual stress. Because the compressive stress is dominant stress, the suspended electrode has a possibility to deflect at this initial position, which means the suspended may not return to the initial position in the following switch on/off working cycles. Compared with the straight state of the axis of the suspended electrode in the initial working cycle, there will be a small deflection as shown in the following figure.

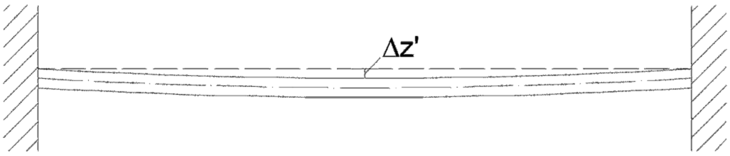

Fig. 18 Switch off position in case of $\sigma_r < \sigma_c$

In the new initial position, the equivalent stress of the suspended electrode will decrease compared with the previous initial position. This is mainly because the deflection of the suspended electrode will introduce an additional tensile stress which is used to balance the thermal compressive stress. However, to determine the initial position of the suspended electrode, many experiments need to be carried out.

Because the thermal compressive load introduces compressive stress, which has a different effect compared with the tensile stress; as a result, the overall minimum stress and overall maximum stress will decrease. The corresponding stress amplitude may keep constant, but the mean stress will decrease significantly. Consequently, the equivalent stress amplitude producing the same damage with null-mean stress will decrease, thereby increasing the number of cycles to failure.

3.2.3 Effects on fatigue limit

Normally, fatigue limits of components are lower at increase temperature.

To study the fatigue behavior of austenitic stainless steel at cryogenic temperatures, several tests have been carried out by using different steels, and these steels present the similar decreased trend of the fatigue strength with the increased temperature [25]. For example, the fatigue behavior of annealed type 347 sheet under fully reversed bending load has been tested with four different temperature, A for 20°C, B for -78°C, C for -196°C, and D for -253°C, respectively. It’s clearly shown that fatigue limits of annealed type 347 sheet have an approximative linear relationship with temperature.

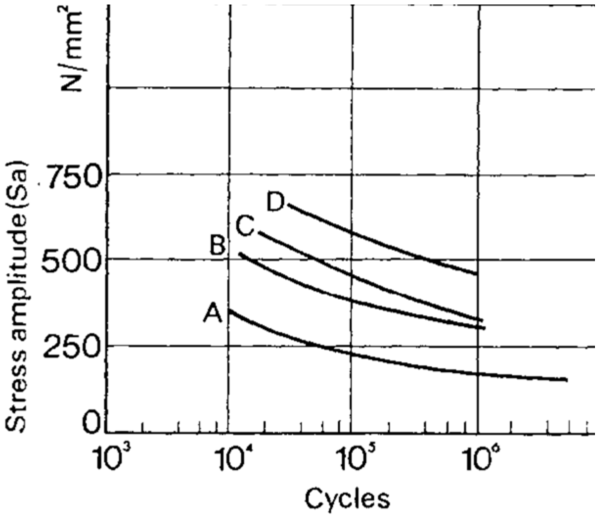

Fig. 19 Temperature effects on the S-N curve of annealed type 347 sheet [25]

The effect of temperature on the fatigue strength of plain weave CFRP was studied. Fatigue tests are conducted at -20°C, 0, 24°C, 100°C and 150°C. It is found that the order of damage events has not changed, but the duration of each event, so the cumulative damage rate is different at different temperatures. It is found that the fatigue life at high temperature decreases with increasing temperature [26].

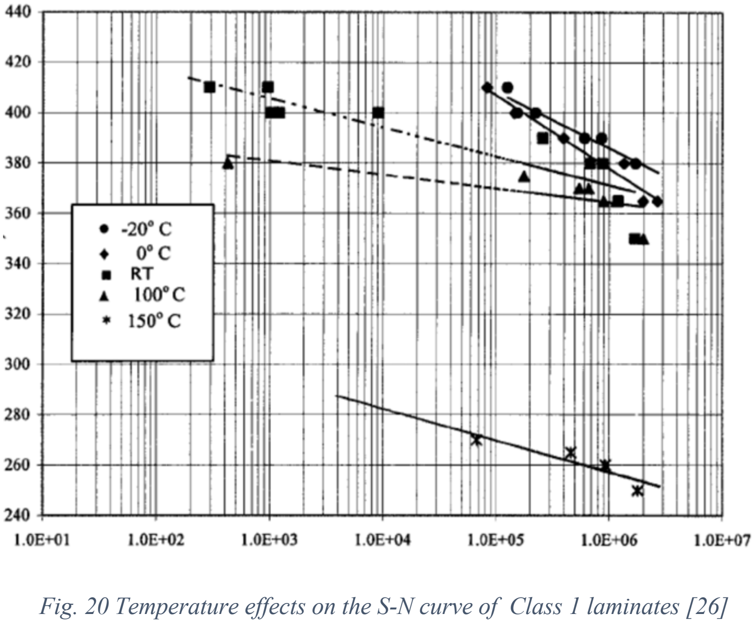

Fig. 20 Temperature effects on the S-N curve of Class 1 laminates [26]

Study of the fatigue results of the two categories at non-ambient temperature shows that the test temperature has a significant effect on the fatigue life of the material. Increasing the test temperature from -20°C to 150°C will greatly reduce the fatigue strength of this composites. Under high stress levels, this reduction in fatigue life is more pronounced, while under low stress levels, this effect gradually weakens. At a stress level of 380 MPa, the fatigue life at 100°C is reduced by more than 2 orders of magnitude compared with room temperature. Compared with 20°C, the lifetime at 100°C is reduced by 3 orders of magnitude. At 150°C, the fatigue resistance is further reduced. The fatigue strength is reduced from 400 MPa at room temperature to 250 MPa at 150°C.

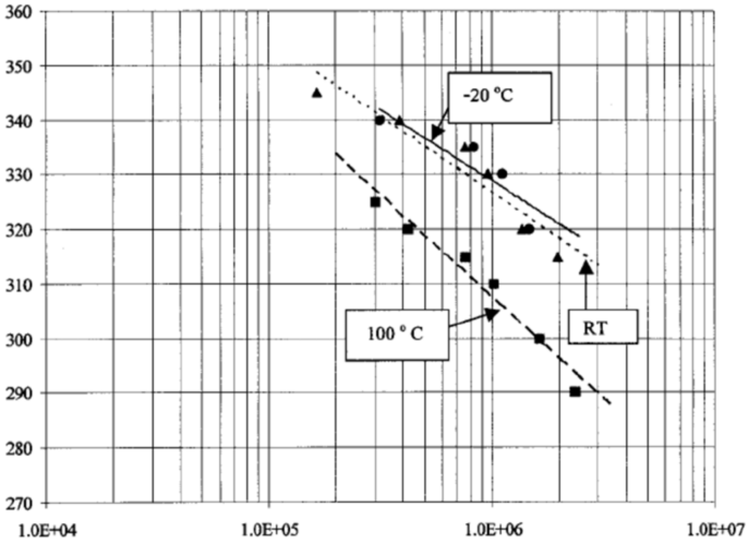

Fig. 21 Temperature effects on the S-N curve of Class 2 laminates [26]

In order to analyze the influence of temperature on the fatigue performance of nickel alloys, especially the influence of low temperature, low-cycle reciprocating beam fatigue tests were carried out on 9% nickel alloy steel samples at 3 different temperatures, including -320F, -110F and 75F [27]. The experimental results clearly show that as the temperature decreases, the fatigue life curve gradually increases.

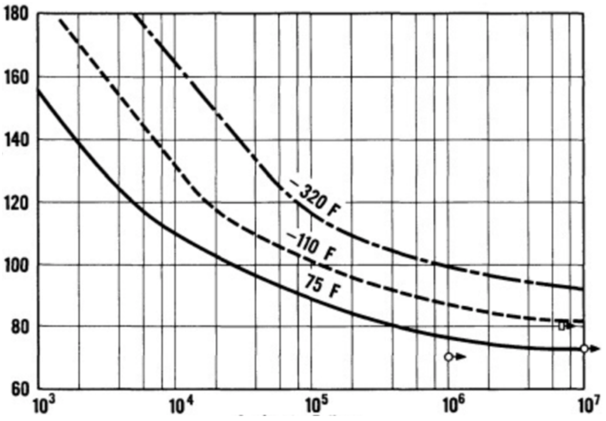

Fig. 22 Temperature effects on the S-N curve of nickel alloy steel [27]

According to FKM theory, there are two temperature ranges related to the correction of fatigue limits, including normal temperature range where no correction is needed and this effect introduced by temperature can be ignored, and high temperature range when correction is an essential part.

For example, normal temperature range used for fine grain structural steel is from -40 to 60°C, for age hardening Aluminum alloys is from -25 to 50°C, for cast iron materials is from -25 to 100°C, and for non-age hardening Aluminum alloys is from -25 to 100°C.

If the temperature is out of the range of normal temperature, the corresponding correction factor need to be considered. According to FKM theory, taking into account different materials, several corresponding formulas are used to correct the fatigue limits. In the following, some formulas for calculating this factor are listed, in which T is in °C.

For fine grain structural steel:

$$K_{T,D} = 1 - 10^{-3} * T \tag{29.}$$

For other kinds of steel:

$$K_{T,D} = 1 - 1.4 * 10^{-3} * (T - 100) \tag{30.}$$

For aluminum alloys,

$$K_{T,D} = 1 - 1.2 * 10^{-3} * (T - 50) \tag{31.}$$

For cast steel, ductile iron, malleable cast iron and gray cast iron, in which coefficient $a_{T,D}$ is 1.2, 1.6, 1.3 and 1.0 respectively:

$$K_{T,D} = 1 - a_{T,D} * 10^{-3} * (T - 100) \tag{32.}$$

Due to the poor adaptability of the gold beam to chemical etching and the defects of the gold beam deformation under residual mechanical stress, Aluminium microbeam and its alloys microbeam are considered as a promising alternative when designing the RF-MEMS.

If we consider Aluminium alloy microbeam used in the RF-MEMS, the formula provided by FKM can determine the temperature coefficient used for modifying the fatigue limit. With this temperature coefficient, the modified fatigue limit $\sigma_{D-1,T}$ can be obtained by the following formula:

$$\sigma_{D-1,T} = K_{T,D} * \sigma_{D-1} \tag{33.}$$

If the operating temperature is located in the range of normal temperature where no correction is needed, the effect of temperature on the fatigue limit can be ignored. The equivalent stress amplitude decreases, the fatigue life increases at the same time. A decrease in the equivalent stress amplitude will lead to an increase in the fatigue life. If the operating temperature is assumed to be 70°C, the corresponding temperature coefficient is 0.976; if the operating temperature is assumed to be 120°C, the corresponding temperature coefficient is 0.916, which means the fatigue limit decreases by 8.4% compared with the standard fatigue limit.

Overall, in the range of normal temperature, the fatigue life of the suspended electrode will increase with the increasing temperature since the thermal compressive stress is introduced. The compressive stress will lower the equivalent stress amplitude, and the fatigue life will increase. If the working temperature is out of range of normal temperature, temperature coefficient needs to be considered. Assume working temperature is 100°C, the corresponding temperature coefficient is 0.94, which means the fatigue limit decreases by 4% only. However, the change in working temperature will introduce compressive stress, which is equal to 109.2 MPa, and the value of this compressive stress is almost equal to 4 times the residual stress. Without considering the buckling phenomenon, as the temperature increases, the equivalent stress amplitude decreases much more than the specific fatigue force, which means that the fatigue life will increase.

4. Damage mechanism of buckling

Buckling is a phenomenon which describes a collapse of structure under compressive load in slender elements, and the main reason is elastic instability. The research on buckling phenomenon can be traced back to the 18th century. The problem of instability was first raised by Euler Bernoulli. The well-known Euler formula theory was obtained, and it is now used to predict the buckling load in linear elastic problems. In the Euler buckling model, the applied load is gradually increased to exceed the critical load, and the buckled structure is obtained from the original configuration.

4.1 Buckling analysis

In order to study buckling, critical load will be introduced which depends on the length of the beam, constraints of the beam, and the second moment of area of the cross section. The following formula is commonly used for calculating critical buckling load.

$$P_{cr} = \frac{\pi^2 * E * I}{(K * L)^2} \tag{34.}$$

In which, P_{cr} which is Euler's critical load, E which is Young's modulus of the beam, I which is the minimum area moment of inertia of the cross section of the beam, L which is the length of the beam, K which is the effective length factor. This effective length factor K changes according to the constraint conditions at both ends of the beam. Generally, the stronger the constraint at both ends, the higher the corresponding critical load.

For load applied which is less than the critical load, the beam will remain straight. The critical load is the maximum load and does not cause buckling. For load applied which is greater than the critical load, the beam will deflect laterally. This critical load makes the beam in an unstable equilibrium state.

According to the clamped-clamped suspended electrode, the corresponding length factor used in our thesis is 0.5, and the corresponding formula is expressed as the following:

$$P_{cr} = \frac{4\pi^2 * E * I}{L^2} \tag{35.}$$

$$I = \frac{W * t^3}{12} \tag{36.}$$

A numerical example will be introduced with the same parameters used in previous examples, in which, the length L of the suspended electrode is 500μm, the width W of the suspended electrode is 35μm, the thickness t of the suspended electrode is 2μm, and the Young's modulus E of the suspended electrode is 69GPa.

Substituting the above values into the formula, the corresponding minimum area moment of inertia of the cross section of the beam is:

$$I = \frac{W * t^3}{12} = 2.3333 * 10^{-11}\ mm^4 \tag{37.}$$

The corresponding critical load is:

$$P_{cr} = \frac{4\pi^2 * E * I}{L^2} = 2.5424 * 10^{-4}\ N \tag{38.}$$

The corresponding critical compressive stress is:

$$\sigma_{cr} = \frac{P_{cr}}{A'} = \frac{4 * \pi^2 * E * I}{L^2 * b * h} = 3.6320\ MPa \tag{39.}$$

4.2 Thermal buckling analysis

When working temperature of the suspended electrode increases, a corresponding thermal load is introduced which has compressive effect on this suspended structure. The following formula has been explained in previous chapter.

$$P_{thermal} = \alpha * \Delta T * E * A' \tag{40.}$$

$$\Delta T = T^* - T_0 \tag{41.}$$

With the formula for calculating critical load P_{cr} , when the thermal load induced by thermal expansion is equal to the critical load, the formula used for determining the critical temperature T^* can be obtained as following:

$$T^* = T_0 + \frac{P_{thermal}}{\alpha * E * A'} = T_0 + \frac{4\pi^2 * E}{\alpha * E * A'} * \frac{W * t^3}{12 * L^2} = T_0 + \frac{1}{3\alpha} * \left(\frac{\pi * t}{L}\right)^2 \qquad (42.)$$

According to this formula, critical temperature T^* only depends on the geometrical parameters of the suspended electrode, including thickness, length, and thermal expansion coefficient. This critical temperature allows us to predict the behavior of the suspended electrode when the working temperature excess this threshold value.

4.21 Thermal buckling analysis without residual stress

In this case, residual stress is not considered, which means the suspended electrode is more likely to present buckling phenomenon. A numerical example is expresses as the following:

$$T^* = T_0 + \frac{1}{3\alpha} * \left(\frac{\pi * t}{L}\right)^2 = 22.5066\ ^\circ\text{C} \qquad (43.)$$

In which, the initial temperature T_0 is set to 20°C. The difference between initial temperature and critical temperature is around 2.5°C, which means a small increase in temperature will active this buckling in absence of residual stress. This result provides that buckling may occur within the operation range of working temperature of the suspended electrode [2].

In order to improve this phenomenon, the geometrical parameters can be modified in the following ways, increasing the thickness of the suspended electrode, decreasing the length of the suspended electrode, using material with lower thermal expansion coefficient. For example, if the length is reduced by half and the thickness is doubled, the corresponding critical temperature is the following:

$$T^* = T_0 + \frac{1}{3\alpha} * \left(\frac{\pi * 2 * t}{L * 0.5}\right)^2 = 60.1051\ ^\circ\text{C} \qquad (44.)$$

After modifying the geometrical parameters, the new critical temperature is three times the previous critical temperature, which means the modified suspended electrode is uneasy to present buckling compared with the previous case. However, in real working condition, the change in length is limited, and an increase in thickness has several significant drawbacks. For example, the stiffness of the suspended electrode becomes higher, and the corresponding applied voltage needs to increase. Besides, the increase in thickness has caused an increase in the use of materials and an increase in weight, which is not in line with the development trend of miniaturization of components. Therefore, it is more important to find a balance between critical temperature and optimization of geometrical parameters.

4.22 Thermal buckling analysis with residual stress

The residual stress state plays an important role in fiber failure in FRML. Marissen (1989) reported that the presence of compressive residual stress in the fiber-binder layer increases the possibility of fiber failure. This is due to residual compressive stress that causes buckling of the fiber and subsequently reduces the fiber's tensile strength. By contrast, the residual tensile stress in the suspended electrode will prevent the phenomenon of buckling to a certain extent, and the main reason is that some of the compressive stress originally used to trigger the buckling is balanced by the tensile stress.

According the previous chapter, in absence of the residual tensile stress, the critical compressive stress is determined which is equal to 3.6320 MPa, and this value allows to determine the stress difference between the residual tensile stress and the compressive stress induced by thermal expansion in the critical condition for buckling. Assume the residual tensile stress σ_r is assumed as 30 MPa, the correspondingly critical compressive stress can be determined as the sum of the residual tensile stress and the stress difference, which is equal to

33.6320 MPa. The corresponding formula for determining the new critical compressive stress is expressed as following:

$$\sigma'_{cr} = \sigma_{cr} + \sigma_r = 33.6320\ MPa \tag{45.}$$

With this new critical compressive stress, the corresponding critical thermal load can be determined as following:

$$P'_{thermal} = \sigma'_{cr} * A' = \ 0.0024\ N \tag{46.}$$

With this critical thermal load, the corresponding temperature difference and corresponding critical temperature can be expressed as following:

$$\Delta T' = \frac{P'_{thermal}}{\alpha * E * A'} = \frac{\sigma'_{cr}}{\alpha * E} = 23.2105\ ℃ \tag{47.}$$

$$T'^{*} = T_0 + \Delta T' = 43.2105\ ℃ \tag{48.}$$

In presence of the residual tensile stress, the new critical temperature is almost twice the previous critical temperature, which means this residual tensile stress can improve the stability of the suspended electrode.

When buckling occurs, the suspended electrode mainly has the following two shortcomings. First, the structure loses its stability, and the straight equilibrium state of the suspended electrode becomes unstable. That is, the deflection caused by any disturbance will not disappear after the disturbance is removed but will continue to expand until it reaches a new state which is far away from the upright state. In addition, the suspended electrode can bend upwards or downwards in this condition; if it bends downwards and the maximum displacement exceeds the gap between the suspended electrode and the fixed electrode, it will directly lead to the spontaneous pull-in phenomenon.

In the following simulation, it's better to determine the testing temperature will not induce the buckling of the suspended electrode, thereby obtaining meaningful analysis results. If the simulating temperature is higher than the critical temperature of buckling, the structure will become extremely complex, and a large number of experiments must be carried out to realize the corresponding analysis and research.

5. Simulation models

The real working condition of the RF-MEMS includes thermal condition, electronic condition, and mechanical condition, which means the most accurate model should be an electro-thermo-mechanical coupling model, thereby analyzing the effect of any parameter changes on the performance of the RF-MEMS. The purpose of this thesis is to study the effect of temperature on the fatigue life of the RF-MEMS, and the following simplified model can be adopted in order to do a preliminary analysis, which is built by the use of COMSOL Multiphysics. Firstly, the electrostatic force is replaced by a prescribed displacement of the center point of the suspended electrode, in which this prescribed displacement is equal to the air gap between the two electrodes. As a result, the stress will differ from the real condition since the area where the electrostatic force applied is the overlap area rather than a single point. Besides, the fixed constraint is set on the two ends of the suspended electrode, in which the stiffness of the anchors' point is as same the center point. In this simulation model, the most dangerous point of the suspended electrode may occur at the center point or at the edge point. In real conditions, the anchors of the suspended electrode consist of two gold layers, which means this part is a harder microstructure, and the most dangerous point of the suspended electrode will be on the center point of the suspended electrode.

W	35	Width of the suspended electrode and fixed electrode [μm]
L	500	Length of the suspended electrode [μm]
t	2	Thickness of the suspended electrode [μm]
g_0	5	Gap height between the suspended electrode and fixed electrode [μm]

Table 9 Geometric parameters of the simulation model

The material used in this simulation model is AA1050 which is provided by the COMSOL material library. The residual tensile stress is 30 MPa. To study the dangerous point at the center area, we will focus on the following three point, including the center point of the upper surface which coordinate is "250μm 17.5μm 2μm", the center point of the lower point which coordinate is "250µm 17.5µm 0µm", and the center point of the body which coordinate is "250µm 17.5µm 1µm". This simulation part will be divided into two parts, the one residual tensile stress higher than the compressive stress, the other residual tensile stress lower than the compressive stress, at the initial position of the suspended electrode.

5.1 Simulation model 1

In this simulation, the range of simulating temperature is from 20°C to 38°C, and in this condition, the residual stress will be higher than the compressive stress induced by the thermal condition. At the initial position, the overall stress is tensile stress during the whole range. With the increase in temperature, the thermal compressive stress becomes higher, and the overall tensile stress becomes lower. If this material used in this simulation is homogeneous, the stresses of these center points are the same, and with the same tensile direction.

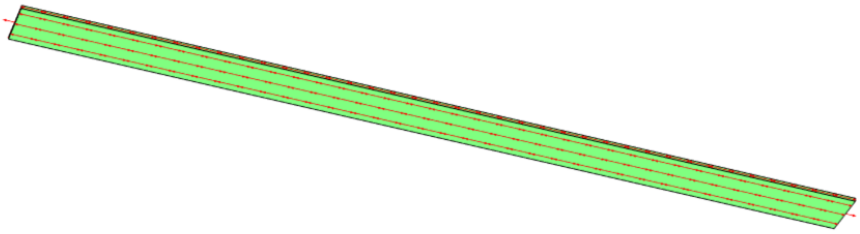

Fig. 23 Stress of the suspended electrode at the initial position, T=20°C

Fig. 24 Stress direction of center points at the initial position, T=20°C

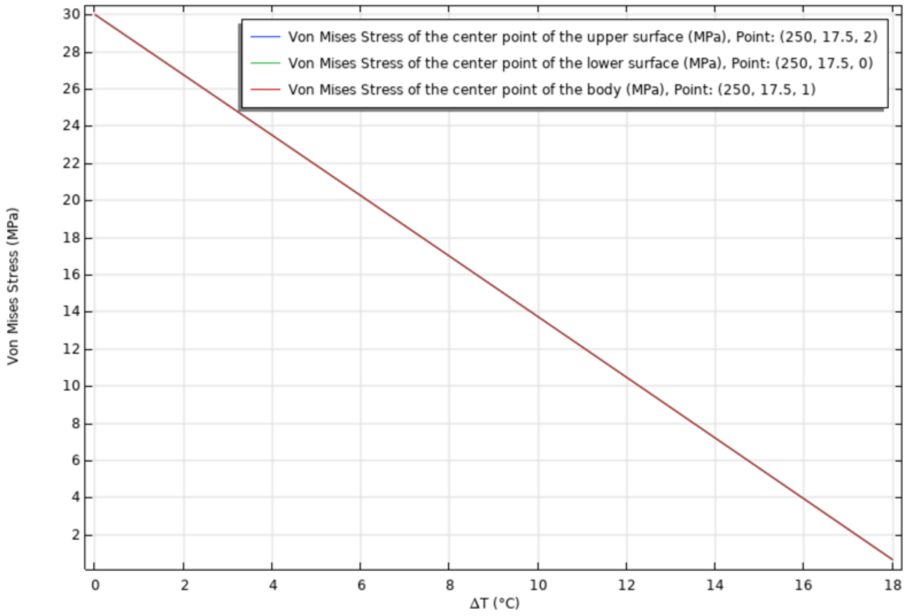

Fig. 25 Stress of center points at the initial position, 20°C<T<38°C

According to these results, it's easy to determine that the stress is equal to 30MPa at 20°C, and the corresponding temperature increase ΔT is 0°C, which means the compressive stress induced by thermal situation is zero. By increasing ΔT, the stress decreases since the compressive stress induced by thermal situation increases. When the temperature increase is around 18°C, which means the corresponding testing temperature is around 38°C, the stress is around 0 MPa, which means the compressive stress induced by thermal situation is equal to the residual tensile stress. At the pull-in position, due to the bending effect, the stresses of the center point of the upper surface, the lower surface, and the body differ from each other. In order to clearly illustrate this temperature effect, the stresses of the suspended electrode at the pull-in position at three different temperature are provided, including 20°C, 30°C, and 38°C.

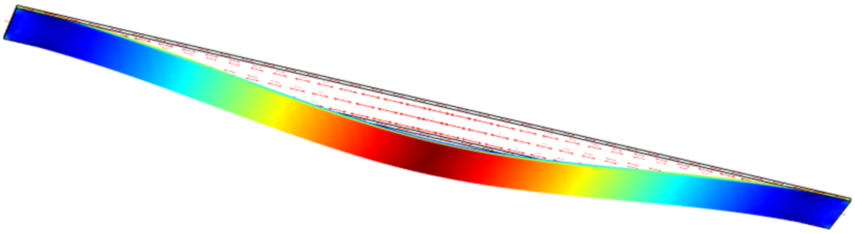

Fig. 26 Stress of the suspended electrode at the pull-in position, T=20°C

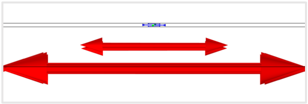

Fig. 27 Stress direction of center points at the pull-in position, T=20°C

Firstly, at this pull-in position, if the testing temperature is 20°C, which means there are no thermal stresses induced, we can determine the stress of the center point of the lower surface is tensile stress, and the stress of the center point of the body is the same tensile stress but is halved. However, the stress of the center point of the upper surface is compressive stress, although the value is close to zero. Therefore, the most dangerous point is the center point of the lower surface.

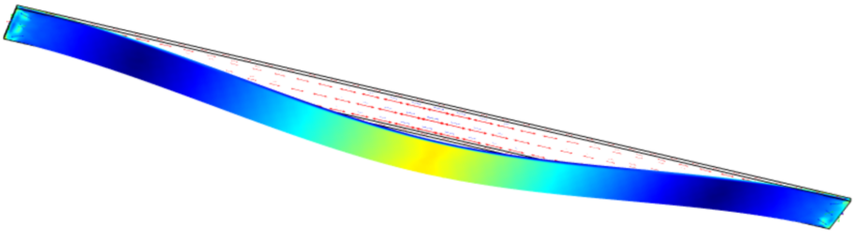

Fig. 28 Stress of the suspended electrode at the pull-in position, T=30°C

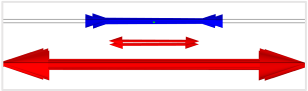

Fig. 29 Stress direction of center points at the pull-in position, T=30°C

Secondly, at this pull-in position, if the testing temperature is 30°C, the tensile stress of the center point of the lower surface decreases due to the present of the compressive stress induced by this temperature increase of 10°C. The tensile stress of the center point of the body shows a similar change. However, the compressive stress of the center point of the upper surface increases since this compressive stress induced by this temperature has the same compressive effect.

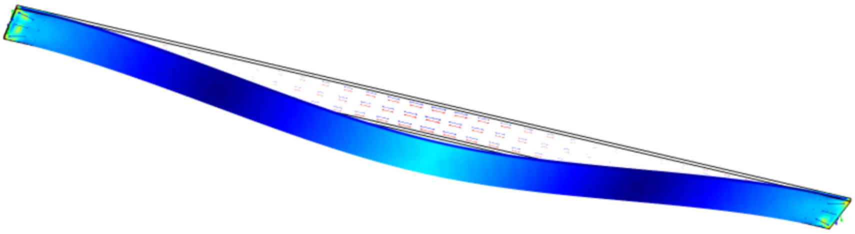

Fig. 30 Stress of the suspended electrode at the pull-in position, T=38°C

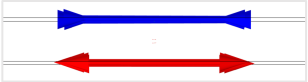

Fig. 31 Stress direction of center points at the pull-in position, T=38°C

Finally, at this pull-in position, if the testing temperature increases to 38°C, which means the compressive effect will be more significant, the tensile stress of the center point of the lower surface continuous to decrease, and the tensile stress of the center point of the lower surface continuous to decrease. It should be noted that the tensile stress of the center point of the body decreases to zero. By contrast, the compressive stress of the center point of the upper surface continuous to increase.

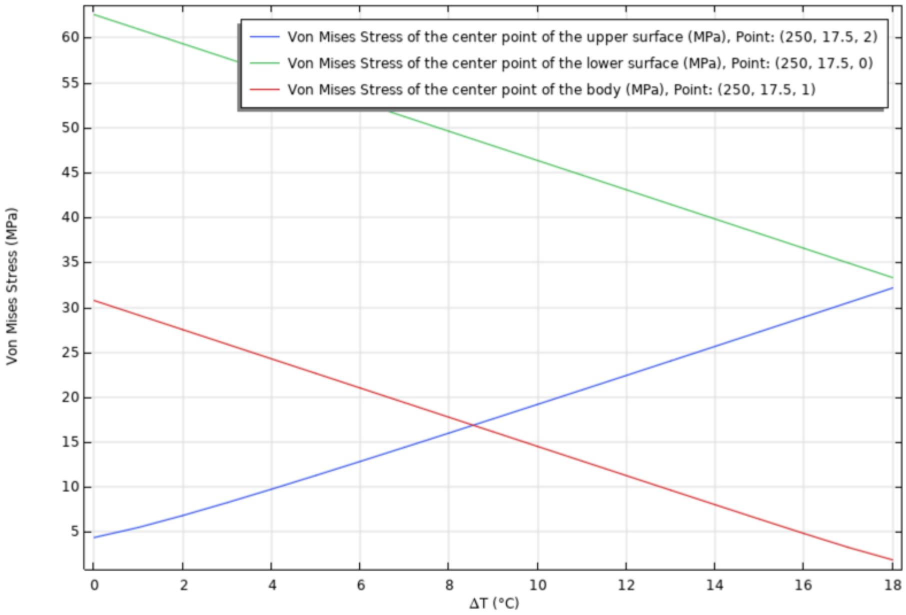

Fig. 32 Stress of center points at the pull-in position, 20°C<T<38°C

According to the reslut during this range of testing temperaure, it's obviously shown that the stress of the center points of the lower surface and the body presents the similar decreasing trend, and the center point of the upper surface showns a contrast trend since this point is always in compression. It should be noted that at the final testing temperature, the stresses of the center point of the upper surface and of the lower surface are very close in number.

stress of the center point at the pull-in position[MPa]				stress of the center point at the initial position[MPa]			
T[°C]	upper surface	lower surface	body center	T[°C]	upper surface	lower surface	body center
20	4.39	62.59	30.77	20	30.00	30.00	30.00
21	5.51	60.97	29.15	21	28.38	28.38	28.38
22	6.84	59.34	27.52	22	26.75	26.75	26.75
23	8.27	57.72	25.90	23	25.13	25.13	25.13
24	9.77	56.10	24.28	24	23.50	23.50	23.50
25	11.30	54.48	22.65	25	21.87	21.88	21.87
26	12.86	52.85	21.03	26	20.24	20.25	20.25
27	14.43	51.23	19.40	27	18.61	18.62	18.62
28	16.02	49.60	17.78	28	16.98	16.99	16.99
29	17.61	47.97	16.15	29	15.35	15.36	15.36
30	19.21	46.35	14.52	30	13.72	13.73	13.73
31	20.82	44.72	12.90	31	12.09	12.10	12.09
32	22.43	43.09	11.28	32	10.45	10.46	10.46
33	24.05	41.46	9.65	33	8.82	8.83	8.82
34	25.67	39.83	8.04	34	7.18	7.20	7.19
35	27.29	38.20	6.43	35	5.55	5.56	5.55
36	28.91	36.57	4.84	36	3.91	3.92	3.92
37	30.54	34.94	3.29	37	2.27	2.29	2.28
38	32.17	33.31	1.90	38	0.63	0.65	0.64

Table 10 Stresses at the pull-in position and the initial position, 20°C<T<38°C

Table 10 lists the minimum stress of center points at the initial position and the maximum stress of center points at the pull-in position. The number in red color means compressive stress, and the number in blue color means tensile stress. Compared with the yield strength of the material of 106 MPa, the stresses at these center points are far less than this yield strength. As a consequence, it can be directly determined that the suspended electrode is in the elastic deformation region. With these minimum stress and maximum stress, the corresponding mean stress, stress amplitude, and equivalent stress amplitude can be determined using the same method in the previous chapter. The previous formula 20, which calculates the equivalent stress amplitude, is available when the mean stress is a positive number. However, with the increase in testing temperature, the compressive stress becomes more and more dominants, which means the mean stress has the possibility to be a negative number.

According to the following Haigh diagram, there are three correlation methods used to consider the effect of mean stress, including linear correlation, modified Goodman correlation, and Gerber parabola correlation [28]. In order to be consistent with the previous discussion, we will use modified Goodman method in this simulation model. With this modified Goodman method, we can reasonably assume that in the safe area on the left, the influence of the mean stress on the fatigue strength can be ignored; in other words, in this area, the equivalent stress amplitude can be directly approximately equal to the stress amplitude. It is worth noting that an increase in temperature will lead to a decrease in the material strength, but compressive stress increases, and operation points migrate from right to left in the Haigh diagram, nevertheless do consider the risk of buckling.

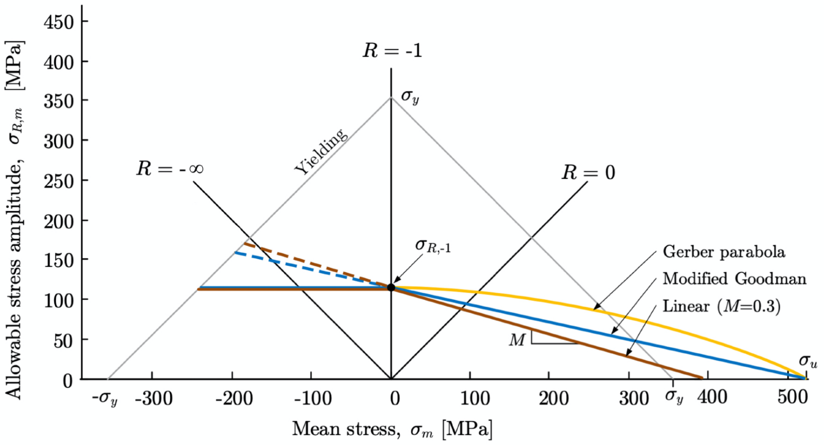

Fig. 33 Haigh diagram showing different mean stress corrections [28]

T[°C]	upper surface center[MPa]			lower surface center[MPa]			body center[MPa]		
	sigma_m	sigma_a	sigma_eq	sigma_m	sigma_a	sigma_eq	sigma_m	sigma_a	sigma_eq
20	12.81	17.19	19.31	46.29	16.29	26.96	30.38	0.38	0.52
21	11.43	16.94	18.78	44.67	16.29	26.36	28.76	0.38	0.51
22	9.96	16.79	18.36	43.05	16.30	25.78	27.14	0.39	0.50
23	8.43	16.70	17.99	41.43	16.30	25.23	25.51	0.39	0.49
24	6.87	16.63	17.67	39.80	16.30	24.70	23.89	0.39	0.49
25	5.29	16.59	17.37	38.18	16.30	24.19	22.26	0.39	0.48
26	3.69	16.55	17.09	36.55	16.30	23.71	20.64	0.39	0.47
27	2.09	16.52	16.82	34.92	16.30	23.24	19.01	0.39	0.47
28	0.48	16.50	16.57	33.29	16.30	22.79	17.38	0.39	0.46
29	-1.13	16.48	16.48	31.67	16.31	22.36	15.75	0.40	0.46
30	-2.75	16.47	16.47	30.04	16.31	21.94	14.12	0.40	0.45
31	-4.37	16.45	16.45	28.41	16.31	21.54	12.50	0.40	0.45
32	-5.99	16.44	16.44	26.78	16.31	21.15	10.87	0.41	0.45
33	-7.61	16.43	16.43	25.14	16.32	20.78	9.24	0.41	0.45
34	-9.24	16.43	16.43	23.51	16.32	20.42	7.61	0.42	0.45
35	-10.87	16.42	16.42	21.88	16.32	20.07	5.99	0.44	0.46
36	-12.50	16.41	16.41	20.25	16.32	19.74	4.38	0.46	0.48
37	-14.13	16.41	16.41	18.61	16.33	19.42	2.78	0.50	0.52
38	-15.77	16.40	16.40	16.98	16.33	19.10	1.27	0.63	0.64

Table 11 Mean stress, stress amplitude, and equivalent stress amplitude, 20°C<T<38°C

According to table 11, in which sigma_m means mean stress, sigma_a means stress amplitude, and sigma_eq means equivalent stress amplitude, it's clearly shown that the most dangerous point is the center point of the lower surface because the equivalent stress amplitude of this point is higher than the stress of the remaining two points, which means this equivalent stress amplitude can determine the fatigue life of the suspended electrode. It should be noted that when the test temperature is higher than 29°C, the mean stress at the center point of the upper surface is a negative number, and the equivalent stress amplitude at this point will be similar to the stress amplitude. Due to the limitation that the experiment cannot be performed at present, the above assupmtion cannot be verified by the experiment for the time being; therefore, we will pay more attention to the fatigue analysis where the mean stress is positive. Fortunately, the mean stress of the center point of the lower surface, which is the dangerous point, is positive.

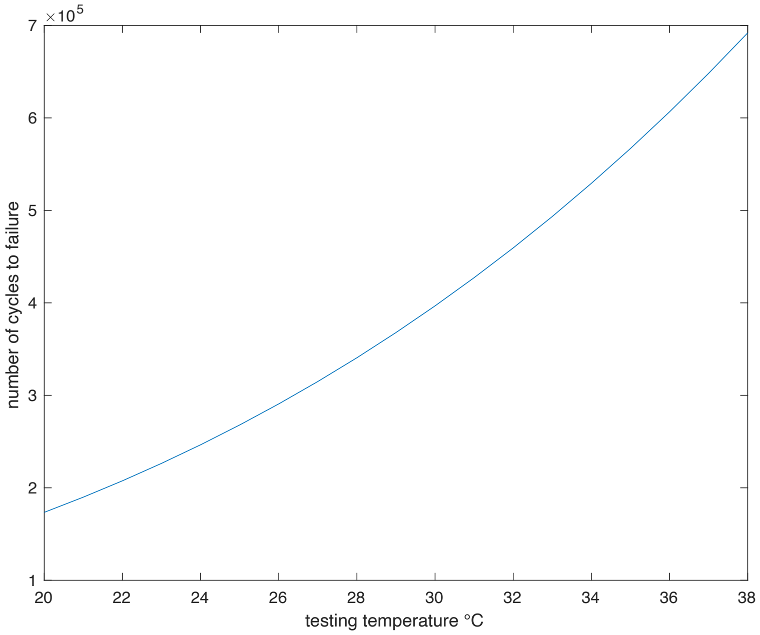

Fig. 34 Relationship between temperature and fatigue life, 20°C<T<38°C

According to figure 34, in the range of testing temperature of 20°C to 38°C, the fatigue life of the suspended electrode increases with the increasing temperature since the thermal compressive stress is introduced and becomes more and more significant. When the test temperature is 20°C, the corresponding fatigue life is 173438; when the test temperature is 38°C, the corresponding fatigue life is 691922. In other words, when the temperature rises by 18°C, the corresponding fatigue life increases by nearly 3 times. This result obtained by this model is very consistent with the theoretical prediction in the previous chapter.

5.2 Simulation model 2

Without taking tests in the lab, it's hard to determine the initial position in real working conditions when the compressive stress is dominant. If we don't set a force to active this deformation at the initial position, the axis of the suspended electrode will remain straight and will not be influenced by the increasing temperature. In this simulation model, the initial position will be assumed as the same in previous simulation model. Although this assumption introduces some errors, this analysis result still has certain guiding significance for future research. In this simulation, the range of simulating temperature is from 38°C to 43°C, and in this condition, the compressive stress induced by the thermal condition becomes the dominant stress because this stress is higher than the residual stress.

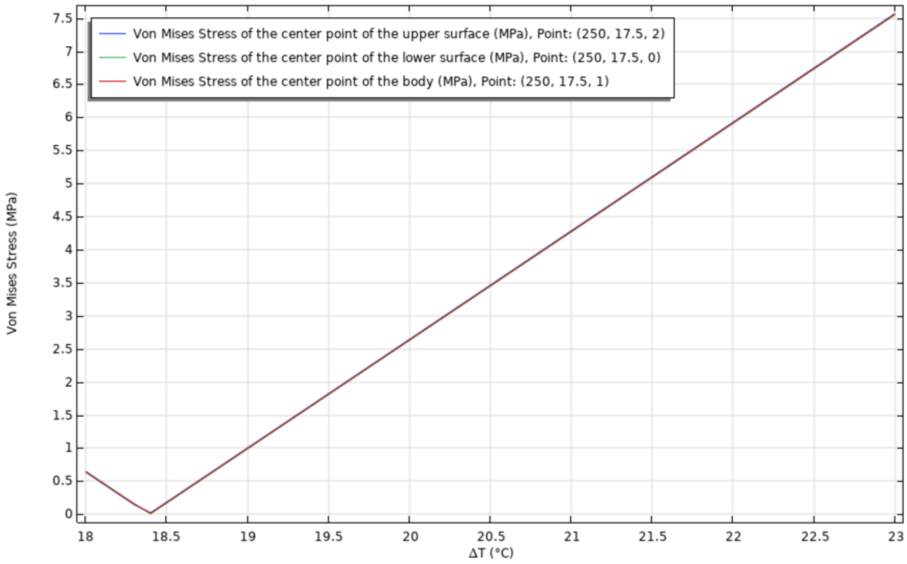

Fig. 35 Stress of center points at the initial position, 38°C<T<43°C

First, the model simulates the initial position. At the beginning of this testing temperature range, the compressive stress is less than the residual stress. At about 38.4°C (ΔT=18.4°C), the compressive stress and the residual stress reach equilibrium, so the equivalent stress is zero; then, as the temperature increases, the compressive stress will be dominate, the corresponding equivalent stress is transformed into compressive stress.

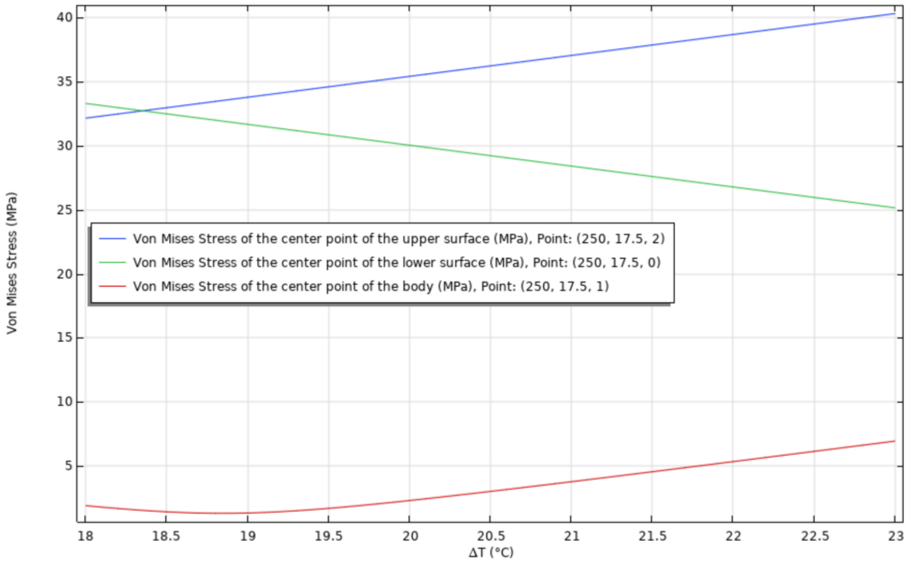

Fig. 36 Stress of center points at the pull-in position, 38°C<T<43°C

Then, the model simulates the pull-in position. It can be clearly seen from the figure that in the entire testing temperature range, the stress at the center point of the upper surface is compressive, and it increases as the temperature rises; the stress at the center point on the lower surface is tensile, and it decreases as the temperature rises. It is worth noting that when the test temperature is about 39°C (ΔT=19°C), the stress state at the center point of the body changes from tensile stress to compressive stress; that is, before 39°C, the stress change trend at this point is the same as the center point of the lower surface; After 39°C, the stress change trend at this point is the same as the center point of the upper surface.

In order to analyze this temperature more clearly, the temperature range is divided into 50 equal parts. The following table 12 lists the minimum stress of center points at the initial position and the maximum stress of center points at the pull-in position, in which the number in red color means compressive stress, and the number in blue color means tensile stress.

stress of the center point at the pull-in position[MPa]				stress of the center point at the initial position[MPa]			
T[°C]	upper surface	lower surface	body center	T[°C]	upper surface	lower surface	body center
38.0	32.17	33.31	1.90	38.0	0.63	0.65	0.64
38.1	32.33	33.15	1.78	38.1	0.47	0.49	0.48
38.2	32.49	32.98	1.67	38.2	0.31	0.32	0.31
38.3	32.66	32.82	1.58	38.3	0.14	0.16	0.15
38.4	32.82	32.66	1.49	38.4	0.02	0.01	0.01
38.5	32.98	32.50	1.42	38.5	0.19	0.17	0.18
38.6	33.15	32.33	1.36	38.6	0.35	0.33	0.34
38.7	33.31	32.17	1.32	38.7	0.51	0.50	0.51
38.8	33.47	32.01	1.30	38.8	0.68	0.66	0.67
38.9	33.63	31.84	1.30	38.9	0.84	0.83	0.83
39.0	33.80	31.68	1.33	39.0	1.00	0.99	1.00
39.1	33.96	31.52	1.37	39.1	1.17	1.15	1.16
39.2	34.12	31.35	1.43	39.2	1.33	1.32	1.32
39.3	34.29	31.19	1.50	39.3	1.50	1.48	1.49
39.4	34.45	31.03	1.59	39.4	1.66	1.65	1.65
39.5	34.61	30.87	1.69	39.5	1.82	1.81	1.82
39.6	34.78	30.70	1.80	39.6	1.99	1.97	1.98
39.7	34.94	30.54	1.91	39.7	2.15	2.14	2.14
39.8	35.10	30.38	2.04	39.8	2.32	2.30	2.31
39.9	35.27	30.21	2.17	39.9	2.48	2.47	2.47
40.0	35.43	30.05	2.30	40.0	2.64	2.63	2.64
40.1	35.59	29.89	2.44	40.1	2.81	2.79	2.80
40.2	35.76	29.72	2.58	40.2	2.97	2.96	2.96
40.3	35.92	29.56	2.72	40.3	3.14	3.12	3.13
40.4	36.08	29.40	2.86	40.4	3.30	3.28	3.29
40.5	36.25	29.24	3.01	40.5	3.47	3.45	3.46
40.6	36.41	29.07	3.16	40.6	3.63	3.61	3.62
40.7	36.57	28.91	3.31	40.7	3.79	3.78	3.79
40.8	36.74	28.75	3.46	40.8	3.96	3.94	3.95
40.9	36.90	28.58	3.61	40.9	4.12	4.11	4.11
41.0	37.06	28.42	3.77	41.0	4.29	4.27	4.28
41.1	37.23	28.26	3.92	41.1	4.45	4.43	4.44
41.2	37.39	28.09	4.08	41.2	4.61	4.60	4.61
41.3	37.55	27.93	4.23	41.3	4.78	4.76	4.77
41.4	37.72	27.77	4.39	41.4	4.94	4.93	4.93
41.5	37.88	27.61	4.55	41.5	5.11	5.09	5.10
41.6	38.04	27.44	4.70	41.6	5.27	5.25	5.26
41.7	38.21	27.28	4.86	41.7	5.43	5.42	5.43
41.8	38.37	27.12	5.02	41.8	5.60	5.58	5.59
41.9	38.53	26.95	5.18	41.9	5.76	5.75	5.75
42.0	38.70	26.79	5.34	42.0	5.93	5.91	5.92
42.1	38.86	26.63	5.50	42.1	6.09	6.07	6.08
42.2	39.02	26.47	5.66	42.2	6.26	6.24	6.25
42.3	39.19	26.30	5.82	42.3	6.42	6.40	6.41
42.4	39.35	26.14	5.98	42.4	6.58	6.57	6.58
42.5	39.51	25.98	6.14	42.5	6.75	6.73	6.74
42.6	39.68	25.81	6.30	42.6	6.91	6.89	6.90
42.7	39.84	25.65	6.46	42.7	7.08	7.06	7.07
42.8	40.01	25.49	6.62	42.8	7.24	7.22	7.23
42.9	40.17	25.33	6.78	42.9	7.41	7.39	7.40
43.0	40.33	25.16	6.94	43.0	7.57	7.55	7.56

Table 12 Stresses at the pull-in position and the initial position, 38°C<T<43°C

With these minimum stress and maximum stress, the corresponding mean stress, stress amplitude, and equivalent stress amplitude can be determined, and the results can be seen in the following table 13.

T[°C]	upper surface center[MPa]			lower surface center[MPa]			body center[MPa]		
	sigma_m	sigma_a	sigma_eq	sigma_m	sigma_a	sigma_eq	sigma_m	sigma_a	sigma_eq
38.0	-15.7662	16.4008	16.4008	16.9795	16.3305	19.1028	1.2665	0.6282	0.6351
38.1	-15.9296	16.4004	16.4004	16.8161	16.3309	19.0721	1.1266	0.6522	0.6586
38.2	-16.0930	16.4000	16.4000	16.6526	16.3314	19.0415	0.9908	0.6802	0.6860
38.3	-16.2564	16.3996	16.3996	16.4892	16.3318	19.0111	0.8599	0.7132	0.7185
38.4	-16.3980	16.4210	16.4210	16.3329	16.3251	18.9738	0.7566	0.7382	0.7430
38.5	-16.5836	16.3984	16.3984	16.1549	16.3327	18.9491	0.6200	0.7975	0.8017
38.6	-16.7470	16.3980	16.3980	15.9915	16.3331	18.9189	0.5097	0.8511	0.8548
38.7	-16.9105	16.3975	16.3975	15.8280	16.3335	18.8888	0.4084	0.9136	0.9168
38.8	-17.0740	16.3971	16.3971	15.6646	16.3339	18.8589	0.3169	0.9860	0.9887
38.9	-17.2374	16.3966	16.3966	15.5011	16.3344	18.8290	-1.0686	0.2356	0.2356
39.0	-17.4009	16.3961	16.3961	15.3376	16.3348	18.7992	-1.1615	0.1645	0.1645
39.1	-17.5644	16.3956	16.3956	15.1741	16.3353	18.7695	-1.2641	0.1031	0.1031
39.2	-17.7279	16.3951	16.3951	15.0106	16.3358	18.7400	-1.3756	0.0507	0.0507
39.3	-17.8914	16.3946	16.3946	14.8471	16.3362	18.7105	-1.4949	0.0061	0.0061
39.4	-18.0549	16.3941	16.3941	14.6836	16.3367	18.6812	-1.6209	0.0319	0.0319
39.5	-18.2189	16.3941	16.3941	14.5201	16.3371	18.6519	-1.7527	0.0642	0.0642
39.6	-18.3824	16.3936	16.3936	14.3566	16.3376	18.6227	-1.8891	0.0916	0.0916
39.7	-18.5459	16.3931	16.3931	14.1931	16.3381	18.5936	-2.0295	0.1152	0.1152
39.8	-18.7094	16.3926	16.3926	14.0296	16.3385	18.5646	-2.1732	0.1356	0.1356
39.9	-18.8730	16.3921	16.3921	13.8661	16.3390	18.5357	-2.3196	0.1532	0.1532
40.0	-19.0370	16.3921	16.3921	13.7026	16.3395	18.5070	-2.4682	0.1685	0.1685
40.1	-19.2005	16.3915	16.3915	13.5390	16.3400	18.4782	-2.6187	0.1820	0.1820
40.2	-19.3640	16.3910	16.3910	13.3755	16.3405	18.4496	-2.7708	0.1940	0.1940
40.3	-19.5276	16.3905	16.3905	13.2120	16.3410	18.4211	-2.9243	0.2046	0.2046
40.4	-19.6916	16.3904	16.3904	13.0484	16.3415	18.3927	-3.0788	0.2140	0.2140
40.5	-19.8551	16.3899	16.3899	12.8849	16.3420	18.3644	-3.2344	0.2225	0.2225
40.6	-20.0187	16.3894	16.3894	12.7214	16.3425	18.3361	-3.3908	0.2302	0.2302
40.7	-20.1827	16.3893	16.3893	12.5578	16.3430	18.3080	-3.5479	0.2371	0.2371
40.8	-20.3463	16.3888	16.3888	12.3943	16.3435	18.2800	-3.7057	0.2434	0.2434
40.9	-20.5098	16.3882	16.3882	12.2307	16.3440	18.2520	-3.8640	0.2491	0.2491
41.0	-20.6739	16.3881	16.3881	12.0671	16.3445	18.2241	-4.0228	0.2544	0.2544
41.1	-20.8375	16.3876	16.3876	11.9036	16.3451	18.1963	-4.1821	0.2593	0.2593
41.2	-21.0010	16.3870	16.3870	11.7400	16.3456	18.1686	-4.3417	0.2637	0.2637
41.3	-21.1651	16.3869	16.3869	11.5764	16.3461	18.1410	-4.5017	0.2678	0.2678
41.4	-21.3287	16.3864	16.3864	11.4129	16.3467	18.1135	-4.6620	0.2717	0.2717
41.5	-21.4928	16.3863	16.3863	11.2493	16.3472	18.0861	-4.8225	0.2752	0.2752
41.6	-21.6563	16.3857	16.3857	11.0857	16.3477	18.0588	-4.9833	0.2785	0.2785
41.7	-21.8204	16.3856	16.3856	10.9221	16.3483	18.0315	-5.1444	0.2816	0.2816
41.8	-21.9840	16.3850	16.3850	10.7590	16.3493	18.0050	-5.3056	0.2845	0.2845
41.9	-22.1481	16.3849	16.3849	10.5954	16.3499	17.9779	-5.4670	0.2872	0.2872
42.0	-22.3117	16.3843	16.3843	10.4318	16.3504	17.9509	-5.6287	0.2898	0.2898
42.1	-22.4758	16.3842	16.3842	10.2682	16.3510	17.9241	-5.7904	0.2922	0.2922
42.2	-22.6394	16.3836	16.3836	10.1046	16.3516	17.8972	-5.9523	0.2944	0.2944
42.3	-22.8035	16.3835	16.3835	9.9410	16.3521	17.8705	-6.1144	0.2966	0.2966
42.4	-22.9671	16.3829	16.3829	9.7774	16.3527	17.8439	-6.2765	0.2986	0.2986
42.5	-23.1313	16.3828	16.3828	9.6138	16.3533	17.8173	-6.4388	0.3005	0.3005
42.6	-23.2949	16.3822	16.3822	9.4507	16.3544	17.7915	-6.6011	0.3023	0.3023
42.7	-23.4590	16.3821	16.3821	9.2871	16.3549	17.7650	-6.7637	0.3041	0.3041
42.8	-23.6231	16.3819	16.3819	9.1234	16.3555	17.7387	-6.9262	0.3057	0.3057
42.9	-23.7867	16.3813	16.3813	8.9598	16.3561	17.7125	-7.0889	0.3073	0.3073
43.0	-23.9509	16.3812	16.3812	8.7962	16.3567	17.6864	-7.2516	0.3087	0.3087

Table 13 Mean stress, stress amplitude, and equivalent stress amplitude, 38°C<T<43°C

According to table 13, it's clearly shown that the most dangerous point is the center point of the lower surface because the equivalent stress amplitude of this point is the highest.

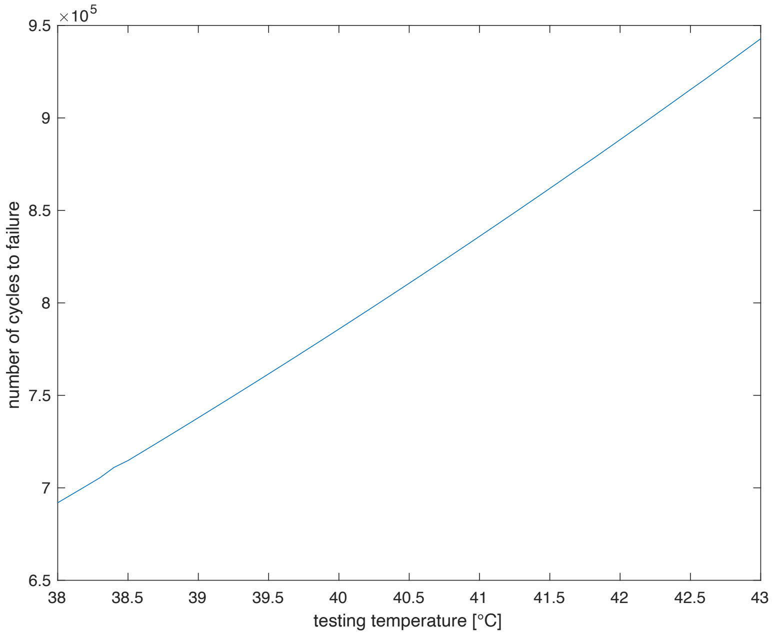

Fig. 37 Relationship between temperature and fatigue life, 38°C<T<43°C

According to figure 36, in the range of testing temperature of 38°C to 43°C, if we don't considet the deflection of the suspended electrode at the initial position, the fatigue life of the suspended electrode increases with the increasing temperature, and this simulation result is very similar to the result of the previous simulation model.

The reason why the simulated temperature stays at 43°C is mainly because if this temperature is the critical temperature of buckling. If the test temperature continues to rise, buckling will occur, making the structure more complicated. As a result, this simulation model will be failed. If the bucking phenomenon is not considered, assuming that the temperature continues to rise, when it reaches a certain value, the compressive stress will be dominate stress at the pull-in position. In this simulation model, when the test temperature is higher than 58°C, the internal stress of the entire suspended electrode will be compressive stress, the corresponding research on metal fatigue analysis caused by pure compressive stress is fewer and fewer, and it is difficult to find corresponding formula models that can be used to predict fatigue.

6. Conclusions

The scope of this work is to propose a method that can predict the effect of temperature on the fatigue life of the suspended electrode. As described in Chapter 1, a detailed analysis of the working principle and manufacturing methods of RF-switch, etc., provides a very useful background knowledge for subsequent analysis. As recorded in the second sheet, a list of available materials and material properties are provided, especially the S-N curves of Au, Cu, Ni and Al. In the third chapter, the stress analysis is carried out firstly, and then the influence of temperature is subdivided into three directions for discussion, including Young's modulus, thermal stress and fatigue strength. It also predicts the influence of temperature on fatigue life. In Chapter 4, the corresponding buckling analysis is provided, and the critical buckling temperature is determined. Finally, the corresponding simulation has been carried out through the simplified model, and the stress that changes with the temperature has been accurately extracted, and the final fatigue life has been calculated; the calculation result of the simulation model is very consistent with the prediction in Chapter 3.

To determine the effect of temperature on fatigue life clearly, this thesis selects a smaller test temperature range to avoid the coupling of buckling phenomena. In this temperature range, Young's modulus decreases as the temperature increases, leading to a decrease in stress; at the beginning of the test, the introduction of thermal stress will offset a part of the residual stress, thereby reducing the total stress; as the test temperature increases, thermal stress becomes the dominant stress, and the resulting compressive stress will move the operating point in the Haigh diagram to the left; due to the low test temperature, the fatigue strength is not affected by temperature. This thesis has determined that in the test temperature range, fatigue life of the suspended electrode increases with the increase of temperature.

In operating conditions, the RF MEMS suffers simultaneously fatigue which is induced by electromechanical excitation, heating effect, surface wear and fretting, thermomechanical fatigue. Besides, the working temperature might cause buckling. To define a suitable thermal condition control requirement and even some requirements in the manufacturing process for residual stress, according to some papers found in the literature a preliminary investigation about the coupling effects among those damage conditions has been developed, by resorting to a simplified analytical approach. This investigation allows comparing the range of temperature compatible with a beneficial effect on fatigue life as well as with the insurgent phenomenon of thermomechanical fatigue and buckling, which are reducing the system life. Further validation of this model must be developed by numerical modeling and through experiments, but unfortunately, the lockdown of cities due to COVID-19 makes it impossible to carry out the experiments.

Acknowledgement

On the completion of the thesis, I would like to thank those who helped me with my graduate study and thesis during this period.

Thanks to Prof. BRUSA EUGENIO and Prof. DELPRETE CRISTIANA for their careful and key guidance during my thesis writing.

Thanks to the hard work of the family, thanks to their considerate support and heart-warming encouragement.

Thanks to my colleagues ZHANG XIU, XIE JIN, LI YIBO, GE LIMENG, and other good friends. Thanks for their more than two years of company with me abroad.

Thanks to all professors who have ever taught me during my graduate study.

Reference

1) Iannacci, Jacopo. "Practical Guide to RF-MEMS". Weinheim: John Wiley & Sons, Incorporated, 2013.

1) Iannacci, Jacopo. "Practical Guide to RF-MEMS". Weinheim: John Wiley & Sons, Incorporated, 2013.

2) E. Brusa, G. De Pasquale and A. Somà, "Experimental Characterization of Electro–Thermo–Mechanical Coupling in Gold RF Microswitches," in Journal of Microelectromechanical Systems, vol. 22, no. 4, pp. 919-929, Aug. 2013, doi: 10.1109/JMEMS.2013.2250486.

3) J. Iannacci et al., "RF-MEMS for 5G mobile communications: A basic attenuator module demonstrated up to 50 GHz," 2016 IEEE SENSORS, Orlando, FL, 2016, pp. 1-3, doi: 10.1109/ICSENS.2016.7808547.

4) K. S. Rao et al., "Design, Modeling and Analysis of Perforated RF MEMS Capacitive Shunt Switch," in IEEE Access, vol. 7, pp. 74869-74878, 2019, doi: 10.1109/ACCESS.2019.2914260.

5) Guisbiers, G. "Materials Selection Procedure for RF-MEMS. " Microelectronic Engineering, 2010.

6) K. Girija Sravani, K. Guha, K. L. Baishnab, G. Shanti and K. S. Rao, "Design of Low Pull-In Voltage and High Isolation of Step Structure Capacitive RF MEMS Switch for Satellite Applications," 2018 IEEE Electron Devices Kolkata Conference (EDKCON), Kolkata, India, 2018, pp. 312-322, doi: 10.1109/EDKCON.2018.8770223.

7) A. Chand, S. M. Ali, S. Mahapatra and A. S. Panda, "Two anchor RF switch with variable step size," 2016 International Conference on Communication and Signal Processing (ICCSP), Melmaruvathur, 2016, pp. 1053-1056, doi: 10.1109/ICCSP.2016.7754310.

8) K. S. Rao, M. D. Prakash and L. N. Thalluri, "Cantilever and circular disc structure based capacitive shunt RF MEMS switches," 2016 International Conference on Electrical,

Electronics, Communication, Computer and Optimization Techniques (ICEECCOT), Mysuru, 2016, pp. 336-338, doi: 10.1109/ICEECCOT.2016.7955241.

9) G. S. Kondaveeti, K. Guha, S. R. Karumuri and A. Elsinawi, "Design of a novel structure capacitive RF MEMS switch to improve performance parameters," in IET Circuits, Devices & Systems, vol. 13, no. 7, pp. 1093-1101, 10 2019, doi: 10.1049/iet-cds.2019.0206.

10) Z. Jiang, Z. Gong and Z. Liu, "Copper-based multimetal-contact RF MEMS switch," 2016 17th International Conference on Electronic Packaging Technology (ICEPT), Wuhan, 2016, pp. 546-550, doi: 10.1109/ICEPT.2016.7583193.

11) Arathy U S and Resmi R, "Analysis of pull-in voltage of MEMS switches based on material properties and structural parameters," 2015 International Conference on Control, Instrumentation, Communication and Computational Technologies (ICCICCT), Kumaracoil, 2015, pp. 57-61, doi: 10.1109/ICCICCT.2015.7475249.

12) B. Jmai, A. Rajhi and A. Gharsallah, "Controllable bridge of the RF-MEMS: Static analysis," 2017 International Conference on Green Energy Conversion Systems (GECS), Hammamet, 2017, pp. 1-4, doi: 10.1109/GECS.2017.8066126.

13) François Cardarelli, "Materials Handbook", a Concise Desktop Reference, 2nd Edition, 2008.

14) E. Brusa, Munteanu, M.G. Role of the electro-thermo-mechanical multiple coupling on the operation of RF-microswitch. Microsyst Technol 18, 983–995 (2012).

15) De Pasquale, G. and Somà, A. “Experimental methods for the characterization of fatigue in microstructures”, Frattura ed Integrità Strutturale, 7(23), pp. Pages 114-126. 2012. doi: 10.3221/IGF-ESIS.23.12.

16) Min, H.-G.; Kang, D.-J.; Park, J.-H. Comparison of Tensile and Fatigue Properties of Copper Thin Film Depending on Process Method. Appl. Sci. 2020, 10, 388.

17) F Sadeghi-Tohidi, Investigation of the effects of extreme stress gradients on fatigue behavior of nickel microbeams [D], Georgia: Georgia Institute of Technology, 2016.

18) Uvarov, I.V., Selyukov, R.V. & Naumov, V.V. Testing of aluminium and its alloys as structural materials for a MEMS switch. Microsyst Technol 26, 1971–1980 (2020).

19) Sakin, Raif. (2016). Fatigue-life estimation and material selection for commercial-purity aluminum sheets. Research on Engineering Structures and Materials. 10.17515/resm2015.30me1205.

20) X Luo, Nonlinear Modeling of MEMS Fixed-Fixed Beams [D], Bethlehem: Lehigh University, 2016.

21) D'Antuono, P, Ciavarella, M. Mean stress effect on Gaßner curves interpreted as shifted Wöhler curves and application to smooth and notched geometries. Fatigue Fract Eng Mater Struct. 2020; 43: 818– 830.

22) Corina, Birleanu & Pustan, M. & Merie, Violeta & Müller, R & Voicu, R. & Angela, Baracu & Crăciun, Stefan. (2016). Temperature effect on the mechanical properties of gold nano films with different thickness. IOP Conference Series: Materials Science and Engineering. 147. 012021. 10.1088/1757-899X/147/1/012021.

23) Olivier Hubert, Xavier Milhet, Pascal Gadaud, Mathieu Tatat, Pierre-Olivier Renault. Modeling of Young's modulus variations with temperature of Ni and oxidized Ni using a magnetomechanical approach. Materials Science and Engineering: A, Elsevier, 2015, 633, pp.76-91. ff10.1016/j.msea.2015.03.014ff. ffhal-01530469f.

24) Hopkins, D.C. & Baltis, Theodore & Pitarresi, James & Hazelmyer, Donald. (2012). Extreme Thermal Transient Stress Analysis with Pre-Stress in a Metal Matrix Composite Power Package. Additional Conferences (Device Packaging, HiTEC, HiTEN, & CICMT). 2012. 000361-000372. 10.4071/HITEC-2012-THA25.

25) McHenry H.I. (1983) The Properties of Austenitic Stainless Steel at Cryogenic Temperatures. In: Reed R.P., Horiuchi T. (eds) Austenitic Steels at Low Temperatures. Springer, Boston, MA. https://doi.org/10.1007/978-1-4613-3730-0_1.

26) Khan, Rehan & Khan, Z.afarullah & Al-Sulaiman, Faleh & Merah, Necar. (2002). Fatigue Life Estimates in Woven Carbon Fabric/Epoxy Composites at Non-Ambient Temperatures. Journal of Composite Materials - J COMPOS MATER. 36. 2517-2535. 10.1177/002199802761405277.

27) Gioielli, P.C., and N. Zettlemoyer. "S-N Fatigue Tests of 9% Nickel Steel Weldments." Paper presented at the The Seventeenth International Offshore and Polar Engineering Conference, Lisbon, Portugal, July 2007.

28) M. M. Pedersen, 2018. Introduction to Metal Fatigue. Department of Engineering, Aarhus University. Denmark. 91 pp. - Technical report ME-TR-11.